Skin-Based Sweat Monitoring Using Radio Frequency Identification Sensors

An honors thesis for the Department of Biomedical Engineering

Lauren E. Klinker

Tufts University, 2012

Acknowledgements

First, I would like to thank Professor Fiorenzo Omenetto for welcoming me into his lab and overseeing this project. Your continuous mentorship has helped me to develop my academic interests through my research and helped me to enjoy the process. I know that this work would not have been possible without your supervision. Thank you.

Thank you to Beibhinn O'Donoghue for working with me over the past year and teaching me about radio frequency measurements and electrical networks. Your guidance was crucial to my successful completion of this project.

I want to acknowledge Isaiah Kacyvenski at mc10, Inc. for inspiring me to work on this project from his personal experience and for bringing the project team together. Additionally, I want to thank Colby Hobart, Conor Rafferty, and Jeffrey Carbeck from mc10 for their expertise shared through our collaboration.

I especially want to thank Professor David Kaplan for advising me over the past four years. You have provided me with a tremendous amount of support in my academic endeavors and led me to so many opportunities. Thank you for all your advice and encouragement.

Thank you to Hu (Tiger) Tao for helping me with scanning electron microscope imaging and data collection from the network analyzer, and to Bob Melville for sharing his knowledge in radio frequency engineering.

Lastly, special thanks to Milva Ricci for your administrative support for this project and to the many other members of the Department of Biomedical Engineering who have assisted me along the way.

Abstract

Wearable sensors are a current trend in personalized healthcare that enable individuals to monitor physiological variables in real-time and without interruption of daily activity. This technology could be beneficial in ensuring the health and performance of athletes, who are at high risk for dehydration due to increased fluid losses through the sweat during training and competition. Even at low levels, dehydration causes excess stress to the cardiovascular system and impairs both physical and cognitive performance. Current methods for monitoring hydration include urine analysis, plasma osmolality, and body mass tracking, yet these methods are limited in their ability to provide information on water and electrolyte losses with instant feedback accessible during activity. This project focuses on the development a wearable device to monitor local sweat losses from the surface of the skin in real-time using a radio frequency identification (RFID) sensor to wirelessly transmit information to a nearby reader. A skin patch for sweat collection was designed by testing the absorption and moisture transmission properties of absorbent cellulose pads and selecting a material to match expected sweat rates without altering secretion from the glands. Subsequently, a passive RFID tag was integrated with the proposed skin patch and the tag antenna was interrogated with a reader during fluid absorption. As conductive fluid accumulated within the patch, an increase in the tag capacitance due to the high dielectric properties of water caused a steady decrease in the center frequency of the reflective power losses. These results demonstrate the ability to detect the volume of conductive fluid collected within an absorbent patch, which could be used to measure the local sweat rate with wireless feedback in real-time. This information could be used to guide fluid and electrolyte replacement to prevent dehydration and maximize athletic performance.

Table of Contents

Index of Figures

Appendix C: Radio Frequency Data

List of Abbreviations

ANOVA ..... Analysis of variance
ASTM ..... American Society for Testing and Materials
C ..... Capacitance
C_F ..... Tag capacitance
Cu ..... Copper
dB ..... Decibels
DPBS ..... Dulbecco's phosphate buffered saline
EAMC ..... Exercise-associated muscle cramp
f_0 ..... Resonant frequency
F_1 ..... Lower cutoff frequency
F_2 ..... Upper cutoff frequency
F_P ..... Maximum frequency of the real impedance
FACSM ..... Fellow of the American College of Sports Medicine
HP ..... Holding power
Hz ..... Hertz
ISM band ..... Industrial, scientific, and medical band
ISO ..... International Organization for Standardization
L ..... Inductance
mM ..... Millimolar
mOsm ..... Milliosmole
mS ..... Millisiemens
MVTR ..... Moisture vapor transmission rate
NaCl ..... Sodium chloride
Q factor ..... Quality factor
R ..... Resistance
R_F ..... Tag resistance
RF ..... Radio frequency
RFID ..... Radio frequency identification
S parameter ..... Scattering parameter
SEM ..... Scanning electron microscopy
TBW ..... Total body water
Z ..... Total impedance

Chapter 1: Introduction

1.1 Significance

"*Minimizing dehydration is the simplest, yet most effective step athletes can take to protect both health and performance.*"

–Bob Murray, PhD, FACSM

Maintaining proper fluid and electrolyte balance is crucial to the overall health and the physical and cognitive performance of the exercising athlete. Electrolytes, the minerals present in all our bodily fluids, are responsible for driving the movement of water throughout our bodies by osmosis. Fluid imbalances occur when electrolyte or water losses through the sweat and urine do not match intake. During exercise, total body sweat losses increase to meet thermoregulatory demands to counteract an increasing core body temperature. When these losses are not replenished, the result is a decrease in plasma volume and increased strain on the cardiovascular and nervous systems. A reduction in total body water of only 1 to 2% of body mass can impair cognitive and physical performance, while serious health risks including death can occur when water losses exceed 7% (Maughan 2003, Wilson 2003). Some of the adverse effects that are marked of various levels of human dehydration are shown below in Figure 1 (Greenleaf 1992, Iowa State University Extension). While by no means exhaustive, this list demonstrates the broad range of physiological changes associated with dehydration.

Just as inadequate fluid replacement can be detrimental to health and performance, excess fluid intake can be equally dangerous to the athlete. Hyponatremia is a condition where the plasma sodium level falls too low from over-consumption of water without also consuming electrolytes. Hyponatremia is most often seen in endurance athletes, such as marathon runners, who drink water in excess of their sweat losses. Early symptoms include dizziness and nausea, and if not detected and treated properly, hyponatremia can cause seizes, collapse, and even death. Dehydration and hyponatremia are serious health threats that must not be ignored. Early

detection and quantification of these exercise-induced fluid imbalances is of paramount importance in order to avoid health risks and performance decrements.

Reduction in Body Mass	Adverse Effects
1%	•Slightly impaired thermoregulation •Decreased physical work capacity
2%	•Thirst response •Vague discomfort
3%	•Dry mouth •Decreased plasma volume •Reduced urine output •Decreased muscular endurance
4%	•Decrease in physical work capacity by 20-30% •Decreased muscular strength •Heat cramping
5%	•Difficulty concentrating •Headaches
6%	•Severely impaired thermoregulation •Increased heart rate •Numbness of extremities
7%	•Severe heat cramping •Delirium •Collapse is likely

Figure 1. The adverse effects of dehydration on athletic performance. Adequate hydration is paramount to the health and performance of athletes. Dehydration by as little as 1-3% total body mass decreases physical performance and can be a significant health risk. (Greenleaf 1992, Iowa State University Extension)

An athlete's hydration level is often monitored by considering three simple markers: urine color analysis, the thirst response, and body mass measurements. While able to track long-term changes in hydration status, these markers are unreliable in terms of providing information on acute changes in hydration due to fluid and electrolyte losses as they cannot be measured without interruption of activity. Additional techniques such as bioimpedance spectroscopy, urine and plasma osmolality measurements, and sweat collection can provide highly accurate data on hydration status at the point of measurement, but they require additional instruments, time, and/or laboratory analysis that are not well-suited for monitoring athletes *in situ*. With the lack of a reliable yet accessible measurement technique to track an athlete's fluid losses in real-time, athletes must estimate their own fluid replacement needs. This often occurs while the athlete is distracted by the on-going game or competition, and the early symptoms of dehydration can easily go unnoticed. Advancement in the tools and techniques available for tracking the athlete's

hydration status and fluid replacement requirements during activity could decrease the prevalence of dehydration and improve the safety of modern athletics.

1.2 Hypothesis and Aims

A skin-based sensor that can quickly and noninvasively quantify the water and electrolyte losses through the sweat could significantly enhance current techniques for the physiological assessment of athletes during competitions. This information is crucial so that the athlete can know the amount and type of fluid that he or she must ingest to maintain proper fluid balance during physical activity and avoid over- or under-consumption. A promising solution is the use of a sweat collection patch integrated with a wirelessly operated radio frequency identification (RFID) sensor.

An RFID system, such as those found in credit cards and anti-theft gates, consists of an RFID tag that is read by a scanning antenna and transceiver to receive and interpret transmitted data. When interrogated by radio waves from a reader, the RFID tag will receive and reflect the incoming waves back to the reader. The reflected data will be affected by the dielectric properties of the local environment, due to resistive and capacitive changes between the antenna coils of the RFID tag. When placed in contact with a skin patch, sweat that has been collected by the patch will affect the radio frequency signal reflected by the tag. In this way, radio frequency interrogation by a reader on the sidelines of an athletic event could provide valuable information on the athlete's sweat losses in real-time, which can be used to inform coaches and training staff on necessary fluid replacement to ensure the health and performance of their players.

The long-term goal of this project is to develop a wearable RFID sensing device that can be used to noninvasively monitor the total sweat and electrolyte losses of athletes during training or competition. ***The goal of this proposal is to determine the feasibility for sweat analysis using***

an RFID tag by characterizing the changes in the resonance response that occur due to the presence of varying levels of water and electrolytes on a skin patch. The hypothesis is that an absorbent skin patch will be capable of collecting sweat over a given skin surface area for analysis with a nearby RFID tag, and that the amount and total ion content of sweat absorbed by the patch will correlate to distinct changes in the resonance behavior of the integrated tag. To test this hypothesis, the following specific aims have been accomplished over the past year:

Aim 1: Determine the material properties of the skin patch components. A skin patch for sweat collection was designed, consisting of an absorbent layer adhered to the skin with a transparent film dressing. This skin patch system must be able to absorb the maximum expected sweat volume over a given area, so that the absorbent layer holds all collected sweat without reaching over-saturation. In addition, sweat absorption from the skin must be rapid so that polymer absorption is not rate limiting and evaporative losses through the skin patch cover must be negligible so that an accurate estimation of sweat losses can be made. It was predicted that thin, non-woven cellulose would meet these requirements as an optimal material for the absorbent layer of the skin patch. The absorptive properties of various cellulose materials were tested using saline solutions with ion concentrations similar to human sweat in order to select a material for use within the skin patch. Once a cellulose absorbent was selected, the electrical properties of the saturated cellulose and the saline solutions were measured and high-resolution imaging was performed to analyze the microstructure of the skin patch materials. This aim provided better understanding of fluid-material interactions within the skin patch, a crucial step prior to the integration of an RF sensor.

Aim 2: Detect fluid volume and conductivity within the skin patch using a radio frequency identification sensor. The next aim was to measure the changes in RFID tag response as

increasing amounts of water and saline solution were absorbed by the skin patch. Specifically, changes in the impedance spectrum of the tag were recorded using a scattering (S) parameter measurement of reflected power. It was expected that changes would be seen in the impedance of the RFID sensor due to the absorption of increasing volumes of water by the polymers and also due to variation in the total ion content different of the absorbed solution. Accomplishment of this aim proved the feasibility of using passive RFID sensing for sweat analysis during collection by a skin patch.

Unpublished work in the Ultrafast Nonlinear Optics and Biophotonics Laboratory has previously demonstrated that RFID sensors could be used to detect changes in salt content and water volume within the vicinity of an RFID tag. With promising preliminary results, our laboratory was well equipped to accomplish the aims presented here to characterize an RFID sensing system for sweat analysis within a skin patch. Next steps on this project will include further testing on an *in vitro* model or on human subjects. The development of an *in vitro* model to simulate sweat secretion through the glands could enhance the characterization of this device prior to use on human subjects. The research proposed here will serve as a foundation for the development of a technique for sweat analysis in real-time that could revolutionize physiological monitoring during athletic competitions.

1.3 Approach Overview

The long-term goal of this work is the development of a wearable skin-based device to accurately monitor the hydration status of the wearer in real-time. The goal of this specific project was to design a skin patch with an integrated sensor for sweat collection and to determine the feasibility of using RFID technology to analyze sweat volume and electrolyte content. A

summary showing the project aims and the parameters measured experimentally can be found in the flowchart shown below in Figure 2.

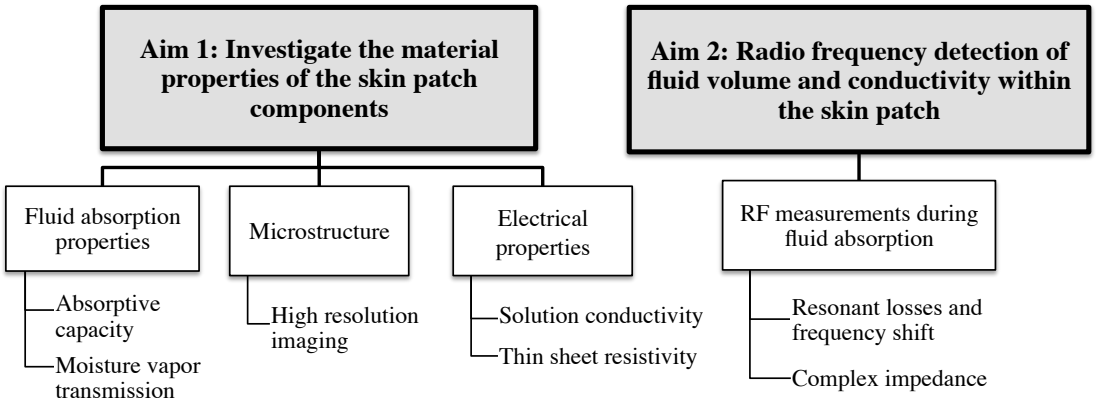

Figure 2. Overall project approach. This chart shows the two project aims as well as the parameters that were measured experimentally. Please refer to Chapter 5: Materials and Methods for a detailed description of all experiments performed.

First, extensive research on the thermoregulatory sweat response and skin physiology was necessary to define a set of design parameters for a skin patch and sensor. The patch must collect all sweat over a defined area without reaching saturation or interfering with sweat secretion from the gland. It was predicted that an absorbent cellulose material would be ideal for collecting and holding sweat in contact with the RFID sensor, and that an additional hydrophilic layer may be necessary for rapid wicking from the skin into the absorbent layer. Lastly, a thin film dressing would be used adhere the patch to the skin. This adhesive layer must be durable to be worn by an athlete for up to 5-6 hours. With this preliminary design, the properties of potential skin patch materials were tested.

Initial experiments focused on measuring the absorptive properties of various grades of thin cellulose pads to be used for sweat collection. For all material tests, de-ionized water and

Dulbecco's phosphate buffered saline (DPBS) containing calcium and magnesium were used. DPBS was chosen because it is similar in ion content to the extracellular fluid, and human sweat is formed from the absorption of ions in the extracellular fluid to yield a less concentrated solution that is secreted through the sweat glands. To create the experimental solutions, DPBS was diluted to a sodium chloride content of 20 to 80 mM using de-ionized water. Dilution was performed based on the physiological sweat sodium concentration because sodium is the most abundant ion found in human sweat. Although lacking minor constituents such as urea, lactic acid, and proteins, these solutions are an adequate sweat model because they are similar to human sweat in terms of electrolyte content, the major sweat component.

Absorption capacity and absorption time were tested first, as the cellulose layer must able to absorb a certain sweat volumes over a small area and the absorption into this layer must not be rate limiting. From these results, the thinnest material capable of absorbing an adequate amount of saline solution was chosen for the absorbent layer of the skin patch. This was done to keep the skin patch less bulky so as to maximize comfort without limiting the athlete's mobility. If cellulose absorption were slower than sweat secretion, alternative materials capable of rapidly wicking sweat from the skin would need to be used so as to prevent reabsorption by the stratum corneum. The next parameter that was examined was the rate of moisture vapor transmission through the skin patch materials. Here, it was important to ensure that water evaporation from the skin patch was minimal so that an accurate measurement of sweat volume could be obtained. Excess evaporative losses would lead to an underestimation of total sweat losses and overestimation of electrolyte content. By measuring the MVTR of these materials, the expected amount of evaporative losses from the skin patch could be estimated. These absorption and evaporation experiments were repeated with de-ionized water and various concentrations of

saline solutions within the physiological range of human sweat (20 to 80 mM sodium) in order to better understand the effect of ion content on the material properties. In addition, high-resolution images of the skin patch materials were taken to visualize the microstructure of the cellulose pads and to estimate the pore size of the thin film cover.

Measurement of sweat volume and electrolyte content using a passive RFID sensor would ultimately rely on changes in the dielectric properties of the absorbent layer of the skin patch. These changes would be caused by the absorption of conductive fluid in the patch. First, the conductivities of the various diluted saline solutions that would be used for radio frequency measurements were measured and recorded. Next, experiments were designed to measure changes in the resistivity of the absorbent cellulose pads following absorption of the saline solutions. The goal of these experiments was to characterize the changes in the electrical resistance of the absorbent pad that occurred upon the absorption of conductive fluid. These results could then be used to better understand any changes in the complex impedance of the RFID sensor.

Once the absorptive and electrical properties of the materials were more thoroughly characterized, one-port reflectance measurements were performed with a network analyzer reader and RFID tag during saline absorption by the skin patch. The coil was placed in contact with a thin film dressing and an absorbent cellulose pad. Changes in the complex impedance of the antenna were measured as the cellulose patch absorbed increasing volumes of saline solution, ranging from 20 mM to 80 mM sodium chloride. For the proposed sweat-monitoring device to simultaneously track both the volume and conductivity of collected sweat, each of these variables must cause distinct electrical changes. Four variables were measured and later analyzed

to distinguish the separate effects of solution volume and conductivity on changed in the tag impedance.

The work described here serves as the basis for future development of a skin-based device for sweat monitoring. By proving the feasibility of this approach for sweat analysis, our hope is to inspire others to continue working towards this long-term goal. An appropriate next step would be the testing of this setup on an *in vitro* model that simulates sweat secretion. Successful detection on an *in vitro* model will lead to device testing on human subjects to collect and analyze actual sweat samples. Further improvements will also include modifications to the antenna coil design for the most sensitive and accurate detection of sweat constituents.

Chapter 2: Background

2.1 Fluid Homeostasis

The human body is comprised of 50 to 60% water by mass, separated into two compartments known as the intracellular and extracellular spaces. The extracellular compartment can be further divided into the interstitial fluid, surrounding all body tissues, and the plasma, which is contained within the vasculature. The intracellular and extracellular compartments hold approximately two thirds and one third of our total body water (TBW), respectively (Hall 2011). The division of body fluid compartments and the approximate percent of TBW in each compartment is shown in Figure 1 (Hall 2011). A healthy physiological state is largely dependent on proper homeostasis or fluid balance between each of the body compartments. Fluid balance is achieved by maintaining adequate overall hydration, or total body water, and a normal electrolyte composition. Electrolytes are charged species that are present in all of our bodily fluids and are responsible for driving the movement of water between fluid compartments by osmosis. Normal concentrations of the major electrolytes found in the extracellular space, intracellular space, and sweat are given in Figure 2 (Maughan 1998). Body water turnover occurs constantly during our daily activities. It is estimated that about 5-10% of our TBW is lost and replaced daily through urine, feces, sweat, and respiration (Maughan 2003). When these water or electrolyte losses are not fully replaced, fluid imbalance will occur.

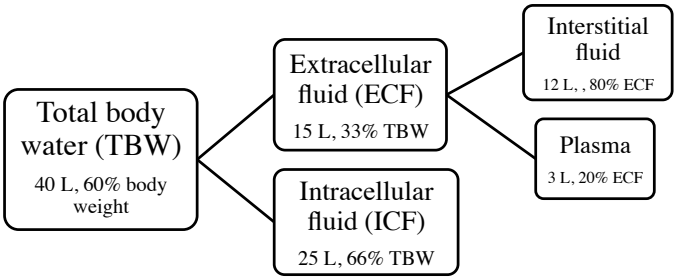

Figure 1. Body fluid compartments. The body is separated into three major fluid compartments. The extracellular compartment consists of the interstitial fluid and the plasma. The approximate volume and percent of TBW contained in each compartment and sub-compartment are shown. (Hall 2011)

	Extracellular Fluid	Sweat	Intracellular Fluid
Sodium	137-144	20-80	10
Potassium	3.5-4.9	4.0-8.0	148
Calcium	4.4-5.2	3.0-4.0	0-2.0
Magnesium	1.5-2.1	1.0-4.0	30-40
Chloride	100-108	30-70	2
Total	280-295	80-160	280-295

Figure 2. Concentrations of major electrolytes in body fluids. All values in mM. These numbers represent the normal physiological ranges for electrolyte concentrations in the sweat, extracellular fluid, and intracellular fluid. (Maughan 1998)

Of healthy populations, athletes are at the greatest risk for developing fluid imbalances due to elevated water and electrolyte losses through the sweat. Sweating is the body's primary mechanism of heat dissipation during physical exertion in hot or humid conditions (Sawka 2007). During physical exertion, sweat rates will increase in order to maintain core body temperature as part of our thermoregulatory system. Evaporation of sweat from the surface of the skin cools the body and protects us against heat illness, which occurs when the body's core temperature rises above the physiological set point due to failure of the thermoregulatory system. If sweat losses are not replenished, diminishing water and electrolyte stores will negatively impact the health and performance of the athlete. Dehydration, or hypovolemia, describes a net loss of body water that is distributed between the different fluid compartments. A diminished plasma volume causes a decrease in the stroke volume of the heart, inducing stress on the cardiovascular system as it tries to maintain adequate blood supply to exercising muscles and to the skin for thermoregulation (Maughan 2003). The heart rate will increase to compensate for a decreased stroke volume by increasing the cardiac output. When the needs of both tissues cannot be met, blood flow to the skin is compromised and the result is a rise in core temperature as the

body struggles to dissipate heat. Under dehydrated conditions, a reduction in skin blood flow is achieved through an increase in peripheral resistance and results in a decreased sweat rate, impairing the body's ability to cool itself (Machado-Moreira 2009). It is estimated that every 1% loss in total body weight increases the core body temperature by .2 to .3 degrees and increases the heart rate by 5 to 8 beats per minute during endurance sports (Coyle 2004). In warm environments, marked by temperatures over 60°F, heat stress exacerbate the body's cardiovascular and thermoregulatory strain in a dehydrated state and core body temperature often rises even higher (Cheuvront 2005).

2.2 Effects of Dehydration on Performance and Health

It has become widely accepted that dehydration by as little as 1-2% of total body mass has a negative impact on physical as well as cognitive performance (Murray 2007, Grandjean, 2007). Perhaps the most evident effect on physical performance is an increased in perceived exertion with increasing levels of dehydration from 2% to 8% during physical activity (Sawka 1999). While numerous studies cite the impairment of aerobic exercise upon dehydration through increased fatigue and work capacity, there is less evidence that dehydration significantly affects anaerobic performance and muscular strength (Murray 2007). In addition to physical performance, research examining the cognitive effects of dehydration have reported impairments in visual-motor tracking, short-term memory, attention, and arithmetic ability at a 2% reduction in total body mass (Gopinathan 1988, Cian 2000). For athletes in an endurance competition or strategizing in a game sport, peak performance is dependent on being properly hydration both before and during the event.

In order to maintain hydration, current guidelines supported by the American College of Sports Medicine recommend that athletes begin hydrating 5-7 mL per kg body weight at least

four hours before exercise and continue drinking enough to replace fluids lost through the sweat (Sawka 2007). Sweat losses vary significantly based on the individual, duration, type, and environment of the activity, but most athletes should be drinking .4 to .8 liters of fluid per hour of exercise. To avoid fluid imbalance, it is also important that the athlete replace electrolytes as well as water, particularly during periods of prolonged exercised. Published guidelines recommend that an athlete ingest fluids containing 20 to 30 millimoles per liter of sodium and 2 to 5 millimoles per liter of potassium throughout exercise for effective electrolyte replacement (Sawka 2007). If salts are ingested in excess of fluid, the athlete may have elevated electrolyte levels in a hypertonic state. Hypertonic hypovolemia is most common seen in athletes exercising for shorter periods of time. This fluid imbalance is brought on by water loss in excess of electrolyte loss, as the sweat is hypotonic to the extracellular and intracellular fluids (Maughan 2003). Similarly, if excess fluid is ingested without salts then the athlete may develop decreased electrolyte levels in a hypotonic state.

One of the most common conditions of electrolyte imbalances seen in endurance athletes is hyponatremia. Hyponatremia is defined by plasma sodium levels of 135 millimoles per liter or less brought on by excess intake of fluid without adequate intake of sodium that is lost through sweat. Hyponatremia poses serious health threats, particularly to endurance athletes such as marathon or Ironman Triathlon participants exercising for over four hours. A recent study conducted at the 2002 Boston Marathon found that 13% of runners had developed hyponatremia according to blood samples collected at the finish line (Almond 2005). Common symptoms of mild hyponatremia include fatigue, muscle weakness, dizziness, nausea, and vomiting, while further decreases in plasma sodium levels can lead to confusion, seizures, loss of consciousness,

and even death (Mayo Clinic). Although a serious health risk, exercise-induced hyponatremia is preventable by adhering to an electrolyte replacement regime during prolonged exercise.

Recent evidence has also linked electrolyte deficiency to the common exercise-associated muscle cramp (EAMC) in the absence of fatigue (Stofan 2005). Exercise-induced dehydration causes body water to redistribute between the fluid compartments, including the movement of extracellular water into the bloodstream to compensate for a decreased plasma volume. This causes the interstitial space to contract in what athletes recognize as a muscle cramp (Bergeron 2008). A study conducted by Stofan and others found that athletes who frequently experience cramping lose twice the amount of sodium through sweating as their non-cramping teammates. Muscle cramping is frequently accompanied by other symptoms of fluid and electrolyte imbalance, including vomiting, nausea, fatigue, dizziness, weakness, and light-headedness (O'Connor 2006). Oral or intravenous replacement of water and electrolytes is usually effective in relieving muscle cramps.

2.3 Current Techniques for Hydration Assessment

With an understanding of the risks associated with exercise-induced fluid imbalance, it is clear that frequent hydration assessment is crucial to ensuring the health and performance of athletes. To maintain body water balance and avoid health threats and impaired performance it is important that the athlete maintain hydration before, during, and after exercise. Thus, a number of techniques have been used to track an individual's hydration level both on and off the playing field. A summary of the most common methods used to assess hydration is given in Figure 3, along with several advantages and disadvantages of each technique (Cheuvront 2005). In this table, various hydration markers are divided into three categories: complex, simple, and other.

The methods shown here vary in their applicability to athletes due to factors such as time constraints, instrumentation requirements, cost, ease of measurement, accuracy, and reliability.

Technique	Advantages	Disadvantages
Complex Markers		
Total body water (dilution)	Accurate, reliable	Analytically complex, expensive, requires baseline
Plasma osmolality	Accurate, reliable	Analytically complex, expensive, invasive
Simple Markers		
Urine concentration	Easy, rapid, screening tool	Easily confounded, timing critical, frequency and color subjective
Body mass	Easily, rapid, screening tool	Confounded over time by changes in body composition
Thirst	Positive symptomology	Develops too late, quenched too soon
Other Markers		
Blood markers: volume, sodium, hormone levels	No advantages over osmolality (except for hyponatremia detection)	Analytically complex, expensive, invasive, multiple confounders
Bioimpedance	Easy, rapid	Requires baseline, multiple confounders
Saliva	Easy, rapid	Highly variable, immature marker, multiple confounders
Physical signs	Easy, rapid	Too generalized, subjective

Figure 3. Summary of current methods for hydration assessment. Plasma osmolarity and total body water measurements are considered the gold standards for determining an individuals' hydration status. (Cheuvront 2005)

When taken together, the two complex markers of plasma osmolality and total body water are considered to provide the gold standard to accurately and reliably diagnose dehydration in a controlled laboratory setting. Measurement of total body water is determined by the dilution technique, where a known amount tracer substance, such as deuterium oxide, is administered orally and allowed to equilibrate between all fluid compartments (Armstrong 2005). After

reaching equilibrium, which usually requires from three to five hours, the amount of the tracer substance found in a body fluid such as saliva or urine is measured. This measurement must be repeated on multiple occasions in order to establish a baseline for each individual. Plasma osmolality is a reliable marker used to detect dehydration when total body water is known, as it is estimated that a 2% loss in body mass causes plasma osmolality to increase by 5 mOsm/kg (Popowski 2001). Although considered an accurate in determining changes in total body water in the laboratory, total body water and plasma osmolality measurements are complex, expensive, and are not reliable measures outside of a controlled setting (Armstrong 2007). Therefore, this technique is not well suited to assess hydration during athletic activities when body fluid compartments are perturbed.

Rather than using plasma osmolality and the dilution technique, hydration is typically assessed in the athlete by using the three simple markers of body mass (weight), urine concentration, and thirst. These markers have been given the acronym as "WUT", and can be used to track day-to-day changes in hydration level according to the diagram shown in Figure 4 (Cheuvront 2005). This technique, endorsed by Gatorade Sports Science Institute, advises athletes to monitor and maintain a constant day-to-day weight, urine frequency and color, and interpret thirst as a sign of dehydration. Warning signs for dehydration include morning weight fluctuations over 1% of total

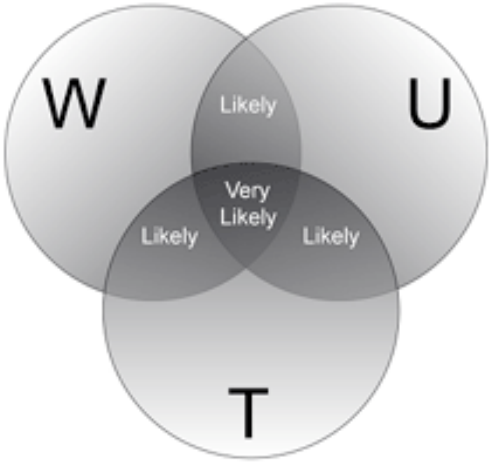

Figure 4. WUT diagram for hydration assessment. The three simple markers of weight (W), urine (U) and thirst (T) can be used for athletes to self-monitor their daily hydration status. The presence of any two of these markers indicates that dehydration is likely, while the presence of all three markers means that it is very likely that the individual is dehydrated. (Photo: Cheuvront 2005)

body mass, reduced urine frequency or darkened urine color, and the presence of thirst. Observing any two of these markers is a likely indicator for dehydration, and observing all three markers indicates that dehydration is very likely (Cheuvront 2005). While this strategy presents a simple and quick way to monitor hydration changes over a period of days to weeks, this assessment technique is highly subjective and not as useful in assessing static or acute changes in hydration status that occur during competition or training.

Some other markers that have been used to assess hydration include blood measurements of plasma volume, sodium, and hormone levels, bioelectrical impedance analysis to determine TBW, measuring saliva flow and osmolality, and observation of physical signs such as dizziness or headache. These markers have been found to be more variable and less accurate at detecting dehydration than the complex markers, but when measured along with the complex markers can present a reliable indicator of hydration status. For example, monitoring urine specific gravity and body mass along with plasma osmolality has been shown to assess progressive changes in hydration status in a laboratory setting with high accuracy (Cheuvront 2010). Bioelectrical impedance analysis and blood measurements require laboratory analysis and can be expensive, while saliva measurements and observing physical signs are not reliable and can be too subjective. While some of these methods have proven useful in determining levels of dehydration in a laboratory setting, many of them are not easily adaptable for everyday use. Effective hydration assessment for the athlete requires a technique that is noninvasive, easy to use, portable and can provide an adequate estimation of hydration status and fluid replacement needs in real-time (Armstrong 2007). This project focuses on investigating the sweat as an alternative physiological marker that can be measured noninvasively and provide information on acute changes in hydration status.

2.4 Sweat Gland Structure and Function

Sweat glands are coiled, tubular structures that originate in the dermal skin layer. There are three types of sweat glands found in humans: apocrine, eccrine, and apoeccrine. The eccrine glands are responsible for thermoregulation and secrete much greater fluid volumes than the apocrine and apoeccrine glands (King 2003). Each eccrine gland consists of a single hollow tubule about 4 to 8 mm long that spans the epidermis and stratum corneum to reach the surface of the skin, where liquid is secreted at the pore (Wilke 2007). As shown in Figure 5, each tubule contains an inner layer of sweat secreting epithelial cells and an outer layer that helps generate the hydrostatic pressure needed to force sweat towards the surface of the skin (Dove 2010). Between two and five million of these glands cover our bodies with an average density of about 200 glands per square centimeter, although some areas such as the palms and the soles of the feet can contain up to 700 glands per square centimeter (Wilke 2007). A higher sweat gland density, however, does not necessarily indicate an increased regional sweat rate during exercise (Smith 2011).

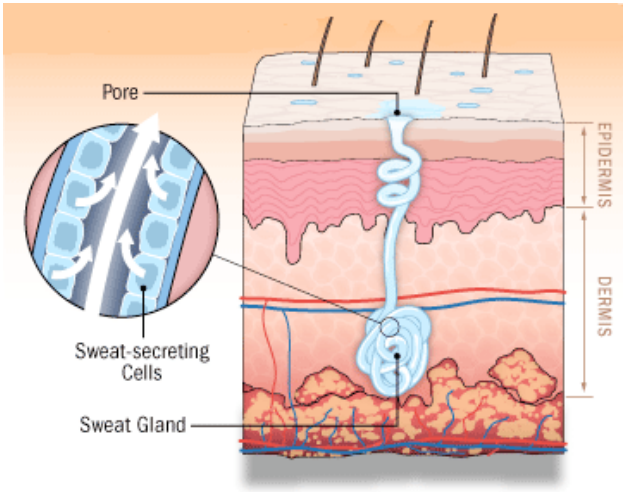

Figure 5. The eccrine sweat gland. The eccrine sweat gland aids in thermoregulation by transporting fluid from the dermis through the epidermis to the surface of the skin. Dissipation of sweat from the pore helps lower the body temperature via evaporation cooling. (Photo: Dove 2012)

The main function of the sweat glands is for thermoregulation. Evaporation of sweat at the surface of the skin dissipates heat to lower the body's core temperature. This process serves as the primary mechanism of thermoregulation during exercise in warm environments (Sawka 2007). Sweat glands respond to sympathetic activation from the hypothalamus in response to an

increase in body temperature above the physiological set point. Sweating can also be caused by an emotional stimulus from the hypothalamus, such as stress, anxiety, or fear. In both cases, cholinergic fibers are responsible for activation of sweat production and secretion at the gland (Wilson 2010). During physical exertion, the highest sweat rates are found at the forehead, neck, anterior and posterior trunk, and lumbar region. The lowest sweat rates are noted at the extremities, side of the chest, and the femoral region (Smith 2011).

2.5 Sweat Losses during Exercise

The sweat is the major route by which the body loses fluid during exercise. Sweat is 99% water but also contains electrolytes as well as small amounts of lactate, urea, ammonia, and proteins. During moderate to strenuous activity, the average person will lose between .8 and 1.4 liters per hour due to sweating, although some individuals can lose up to 3 liters per hour during prolonged exercise in the heat (Nadel 1980). Sweat rates will increase to meet the thermal load on the body, unless dehydration ensues and the thermoregulatory demands can no longer be met. The thermal load alone, however, cannot be used to accurately predict an individual's sweat rate. Instead, the sweat rate is influenced by a number of environmental factors, such as the humidity, wind conditions, and ambient pressure, and individual factors, such as heat acclimation, fitness level, clothing, and size (Cheuvront 2007). Human sweating is a complex process, and many factors must be considered in order to accurately estimate sweat rate for a given exercise and duration.

Sweat rate determination is important because if water and electrolytes lost through the sweat are not adequately replaced then the athlete is likely to develop fluid imbalance. Thus, the American College of Sports Medicine recommend that athletes aim to completely replace all water and electrolytes lost through the sweat (Sawka 2007). The electrolyte content of sweat,

however, varies widely between individuals and also between different body locations. Sodium, the main cation found in sweat, is usually present between 20 and 80 millimoles per liter while chloride, the major anion, is found between 30 and 70 millimoles per liter (see Figure 2, above). Small amounts of potassium, calcium, and magnesium are also present. Recent studies have examined the variation in electrolyte content based on body location by comparing the concentrations of ions in whole body sweat losses and regional collection (Baker 2009, Patterson 2000). Patterson and colleagues found that sweat samples taken from the thigh, foot, and lower back most closely correlated to total body sodium and potassium losses, while Baker and others found the thigh and chest to be the best predictors.

At low levels of physical activity and under proper heat acclimation, sweat will be hypotonic relative to the extracellular and intracellular fluid compartments. Once stimulated, the gland will produce primary sweat that is isotonic to the extracellular fluid. Primary sweat enters the sweat glands within the dermal layer, and electrolyte reabsorption will occur along the epithelial cells as sweat moves towards the epidermis and stratum corneum for secretion. This process of reabsorption conserves the body's electrolyte stores. As the thermoregulatory response intensifies to meet the demands of prolonged or high intensity exercise, however, sweat rates will increase and electrolyte reabsorption along the duct will no longer be able to keep up with the rate of secretion. When this happens, increased concentrations of electrolytes will be excreted and the sweat composition will approximately match that of the extracellular fluid (Patterson 2000). The reabsorption mechanism is better able to keep up with sweat production in an individual who is heat acclimated and well trained in the activity being performed (Ichinose-Kuwahara 2010). If the osmolarity of the extracellular fluid changes significantly, such as in hypertonic hypovolemia, then this change should be reflected by a similar change in the sweat

osmolarity. In a recent study by Morgan et al., the osmolarity of sweat collected at the forearm increased under a hypertonic dehydrated state as compared to a fully hydrated state (2004). In this study, sweat osmolarity was found to increase from 160 mOsm/L to 172 mOsm/L due to increases in sweat sodium and chloride losses over two hours of heavy exercise. For well-trained, heat acclimated individuals, however, sweat reabsorption processes are more efficient and dehydration may ensue without an elevation in sweat osmolarity.

2.6 Current Techniques for Assessing Sweat Loss

Sweat monitoring is a valuable tool that could be used to help prevent fluid imbalance and muscle cramping by dictating an individual's water and electrolyte replacement needs during exercise. When analyzed along with other variables, information on the volume and osmolarity of excreted sweat could be used to more accurately assess acute changes in hydration status. Current techniques for sweat analysis examine either whole-body or regional sweating, and require post-collection laboratory processing to determine a) the volume of sweat loss by change in mass and b) the amount of electrolytes lost. Considering whole-body sweating, the sweat rate can either be calculated after tracking changes in body mass while accounting for the intake and secretion of any fluids, or the amount of sweat can be measured directly by the whole body wash down technique. In the whole body wash down technique described and tested by Shirreffs and Maughan, the participant cycles in an area confined by pre-cleaned plastic materials (1997). Upon completion of exercise, the participant washes him or herself thoroughly inside the confined area with a known amount of water. The volume of liquid left in the confined area is then measured and the sweat volume can be determined from a dilution calculation (Shirreffs 1997). This technique has been shown to provide accurate and reliable measurements of both sweat volume and electrolyte content, but requires a highly controlled laboratory setting (Baker

2009). Rather, regional sweat collection is considered a much more practical method for use by athletes in the field.

Regional sweat collection can be performed at a single site or at multiple sites on the body. Techniques for regional sweat collection include an absorbent pad attached to the skin, the Macroduct sweat collection system, or the ventilated-capsule method. The Macroduct system consists of a plastic capsule that forms a tight seal against the skin. Sweat is collected up into the plastic via capillary tube action under hydraulic pressure (Hammond 1993). This method was originally developed for use in the pilocarpine test for cystic fibrosis, in which sweat glands are stimulated by iontophoresis and the sweat chloride content is measured. An alternative technique is the ventilated-capsule method, in which nitrogen gas is sent through a capsule attached to the skin at a fixed rate. The change in humidity of the nitrogen gas flowing through the capsule is measured by a hygrometer to determine the sweat losses (Kondo 2001). Following regional collection by one of these techniques, ion chromatography, flame photometry, or atomic absorption spectrometry is used to determine the sweat electrolyte content.

Because sweat rates vary widely at different body regions during exercise, weighted equations are often used to estimate whole body sweat volume and electrolyte losses from data collected at various sites, often at the forearm, back, chest, thigh, or forehead. A table providing sweat rate data at these five locations taken from relevant literature is shown in Figure 6. Once the local sweat rate at these locations has been determined experimentally, total body sweat losses can be estimated by multiplying the local sweat rate by the individual's body surface area. Recent studies have shown that collection at certain locations can be used to accurately predict whole body total sweat losses, while other locations repeatedly over or underestimate whole body sweat volumes. Thus, appropriate sweat patch placement is crucial to collect meaningful

data on total sweat losses. It has been found that the mid-anterior thigh, gluts, and lateral mid-chest showing the strongest correlation to the average whole body sweat rate at two exercise intensities (Smith 2011). The thigh is the only body location for regional collection that has been shown to correlate well with both whole body sweat rate as well as electrolyte content (Smith 2011, Patterson 2000).

Body Location	Collection Area	Sweat Rate (mL/cm^2•hr)	Author, Year
Forehead	36 cm^2	.066-.246	Bain, 2011
	42 cm^2	.09 (mean)	Baker, 2009
	8 cm^2	.1434 (mean)	Patterson, 2000
	56 cm^2	.0188-.3262, .0697 (median, low intensity), .1710 (median, high intensity)	Smith, 2011
Chest	42 cm^2	.036 (mean)	Baker, 2009
	5.2 cm^2	.018-.066	Buono, 2007
	372 cm^2	.0191-.0744, .0244 (median, low intensity), .0390 (median, high intensity)	Smith, 2011
Forearm	64 cm^2	.0132-.054	Bain, 2011
	42 cm^2	.036 (mean)	Baker, 2009
	5.31 cm^2	.006-.042	Kondo, 2001
	24 cm^2	.045 (mean)	Patterson, 2000
	644 cm^2	.0106-.0487, .0266 (median, low intensity), .0372 (median, high intensity)	Smith, 2011
Lower Back	42 cm^2	.048 (mean)	Baker, 2009
	24 cm^2	.051 (mean)	Patterson, 2000
	167 cm^2	.0294-.2094, .0677 (median, low intensity), .0856 (median, high intensity)	Smith, 2011
Thigh	42 cm^2	.024 (mean)	Baker, 2009
	24 cm^2	.0396 (mean)	Patterson, 2000
	736 cm^2	.0150-.0607, .0271 (median, low intensity), .0370 (median, high intensity)	Smith, 2011

Figure 6. Regional sweat rates by body location. Sweat rates determined experimentally by regional collection at the forehead, chest, forearm, lower back, and thigh are given. The thigh and chest have been shown to be good predictors of total sweat losses during exercise when adjusted for total body surface area (Smith 2011).

While these current methods for regional and whole body sweat losses can provide highly accurate and sensitive measurements of ion concentrations, they require laboratory instrumentation and produce one-time measurements that cannot provide data on sweat losses in real-time. With this in mind, the project aims to develop a wearable and noninvasive device to collect and analyze the sweat in real-time, so that the athlete, coaches, and training staff may access this information quickly during a game or event. Such a device will provide data on both the volume of water and the amount of electrolytes lost through the sweat in order to inform the athlete on 1) the amount of water and electrolytes that should be replenished and 2) his or her current hydration status. This device must have high sensitivity to detect changes in total sweat osmolarity of about 5 millimoles per liter. To achieve this sensitivity and a high level of accuracy in a quick measurement, the use of radio frequency technology is proposed.

2.7 Radio Frequency Identification Sensors

Radio frequency identification (RFID) technology is used for wireless data tracking in countless application, including credit cards, patient wristbands in hospitals, timing chips during road races, anti-theft gates in stores, and more. RFID tags can be separated into two major categories of active or passive devices. A passive RFID tag has no power source, and is driven by a reader to transmit information. An active RFID tag contains a power source and can therefore power the tag circuit and antenna to transmit information. Passive RFID tags are chosen as an ideal signal transduction mechanism in a wearable device such as a sweat indicator because they are simple, inexpensive, and can be incorporated into a wireless system for measurements with a reader and antenna. Radio frequency (RF) communication between a tag and reader is diagrammed in Figure 7 (Dobkin 2008). When interrogated with an electromagnetic field by a reader antenna, the RFID tag will produce a voltage that is reflected as a backscattered

signal to the reader. This measurement uses the scattering (S) parameter, which is a measurement of power transmitted between a tag and reader. In the S11 parameter, the power reflected from a single port on a network analyzer to a passive load is measured.

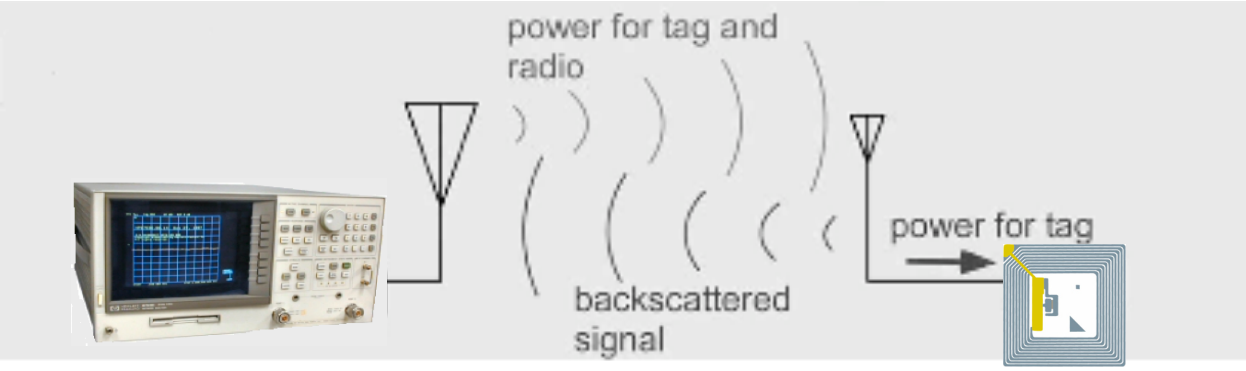

Figure 7. Radio frequency reflectance measurements. A reader, such as a network analyzer (left), transmits an electromagnetic field which powers a tag (right). A high voltage is generated in the tag and reflected back to the reader as a backscattered signal. (Photo: Dobkin 2008)

In addition to radio communications, recent work has shown that passive RFID tags can also be used to detect changes in the local environment. Chemical species surrounding the tag will affect the reflective losses in the backscattered signal in an S parameter measurement. This has been demonstrated by the ability of RFID tags to detect and quantify chemical analytes in air as well as the conductivity of buffered solutions (Potyrailo 2010). When a material comes in contact with an RFID tag, the dielectric constant between the antenna turns will be altered. This will cause a change in the tag resistance (R_F) and capacitance (C_F), as shown in Figure 8 (Potyrailo 2009). These changes will alter the complex impedance of the RFID tag when interrogated by a reader through inductive coupling. If a skin patch is placed in contact with a passive RFID tag, sweat collected in the patch should cause detectable changes in the impedance spectrum of the antenna. In this way, an RFID sensor could potentially be used to monitor regional sweat losses from the surface of the skin in real-time. Information on the athlete's sweat

losses could be obtained by a single swipe of a handheld reader over an RFID tag integrated within a skin patch. The development of such a wearable, RFID sensing device for sweat monitoring is the long-term goal of this project.

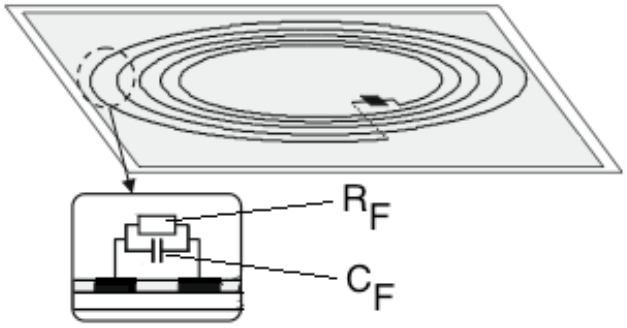

Figure 8. RFID tags as sensors. Changes in the dielectric constant between adjacent coils on an RFID tag can be used to detect environmental conditions or the presence of chemical species. Above is a passive RFID tag showing the resistive (R_F) and capacitive (C_F) elements between each of the antenna turns. (Photo: Potyrailo 2010)

Chapter 3: Results

3.1 Conductivity of Saline Solutions

Thirteen saline solutions varying in ion content within the physiological range of human sweat were prepared from Dulbecco's phosphate buffered saline (DPBS) for use in all material absorption tests and radio frequency measurements. These solutions ranged from 20 mM sodium chloride to 80 mM sodium chloride, with each solution differing by 5 mM. A list showing the sodium chloride content, conductivity, resistivity, and total osmolarity of each experimental solution is provided below, in Figure 1. Conductivity was measured directly using a probe, while resistivity was calculated as the inverse of conductivity and total osmolarity was calculated based on the dilution factor. Conductivity did not vary with volumes of solution up to 150 mL.

NaCl content (mM)	Conductivity (mS/cm)	Resistivity (Ω•m)	Osmolarity (mOsm/L)
0 (DI water)	1.24×10^{-3}	8060	0
20	2.47	4.05	41.33
25	3.16	3.17	51.63
30	3.69	2.71	61.99
35	4.29	2.33	72.32
40	4.96	2.02	82.65
45	5.66	1.77	92.98
50	6.12	1.63	103.31
55	6.91	1.45	113.65
60	7.22	1.39	123.98
65	7.69	1.30	134.31
70	8.45	1.18	144.64
75	8.78	1.14	154.97
80	9.32	1.07	165.30
137.93 (undiluted DPBS)	16.43	.609	285

Figure 1. Properties of experimental saline solutions. Thirteen solutions varying in ion content with the normal physiological range of human sweat (~20 to 80 mM sodium) were prepared by diluting Dulbecco's phosphate buffered saline (DBPS) containing calcium and magnesium with de-ionized (DI) water. Conductivity was measured with a conductivity probe, and resistivity and osmolarity were later calculated.

3.2 Cellulose Absorption

To select an appropriate material for the absorbent layer of the sweat patch, nine types of absorbent sheets made from 100% cellulose fibers were tested for their fluid absorption properties. These pads differed in thickness as well as pore size (see Chapter 5, Figures 1 and 2). The absorption capacities of the cellulose sheets were measured by immersing each material in saline solution for various durations. To avoid saturation under maximum sweat rates on the thigh for up to three hours of wear, the selected cellulose material must be able to absorb at least 4.5 mL of solution over the patch area of 25 cm^2. Four grades of absorbent cellulose, 900 and 300 from GE Whatman™ and 197 and 165 from Pall Corporation, met the required absorption capacity following 10 seconds and 6 hours of saline immersion. The average amount of saline absorbed by each grade of absorbent cellulose after 10 seconds of immersion and 6 hours of immersion in 50 mM sodium chloride saline are shown below in Figure 2. Differences in absorption capacity between the nine grades varied significantly at both time points based on a 1-way unpaired analysis of variance (ANOVA) with a 95% confidence interval ($p<.0001$). These experiments also revealed that saline absorption by cellulose occurs rapidly, as samples reached between 77.7% (grade CF3) and 94.9% (grade 197) of maximum absorption after 10 seconds of immersion.

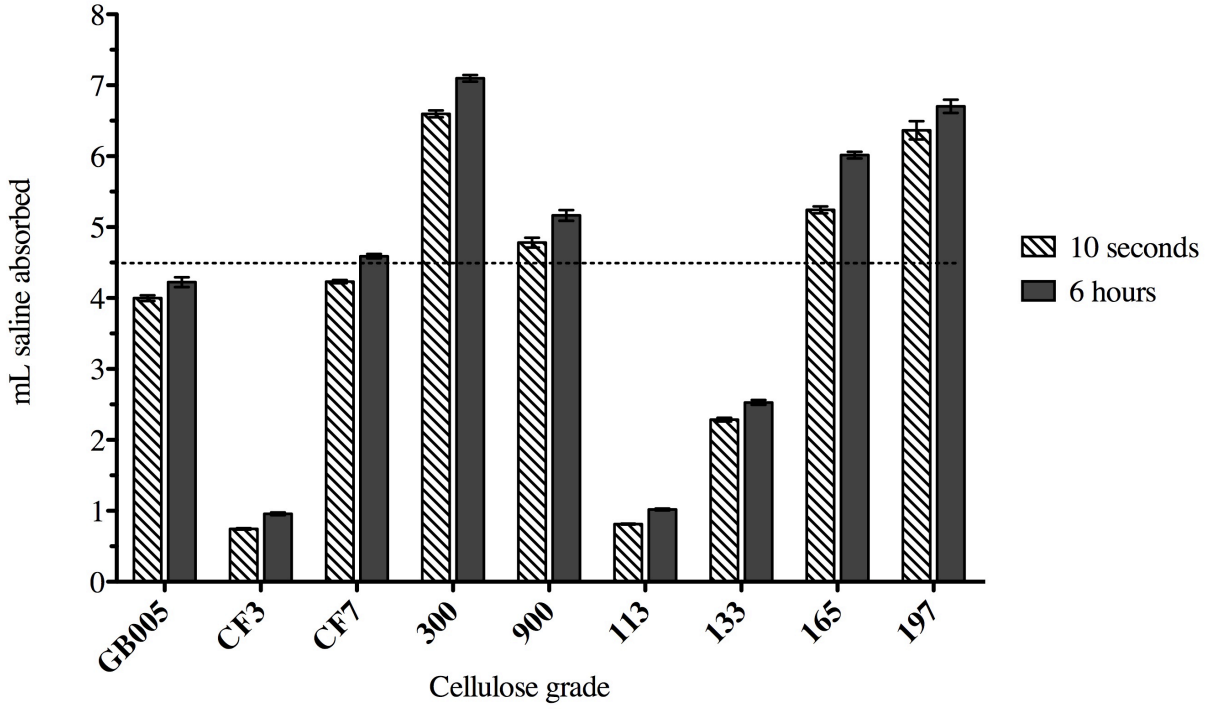

Figure 2. Amount of saline absorbed by cellulose pads. The total amount of 50 mM sodium chloride saline absorbed by cellulose pads after 10 seconds and 6 hours of immersion are shown. Grades 300, 900, 165, and 197 met the absorption requirement of 4.5 mL at both time points. Mean values ± standard error are given for n=6 samples. Absorptive capacity between the material grades varied significantly at both 10 seconds and 6 hours (1-way ANOVA, p<.0001).

The maximum absorption capacity expressed as the percent increase in mass following saline immersion was calculated for each material grade. Variation in the percent increase in mass was significant for the nine grades of cellulose absorbent sheets based on a 1-way unpaired ANOVA (Figure 2, p<.0001). Figure 3, below, shows the percent increase in mass for each of the nine cellulose materials after immersion in saline solution diluted to 50 mM sodium chloride for 6 hours. Grade 165 from Pall Corporation achieved the greatest percent increase in mass, absorbing 534.98± 7.43% its original mass.

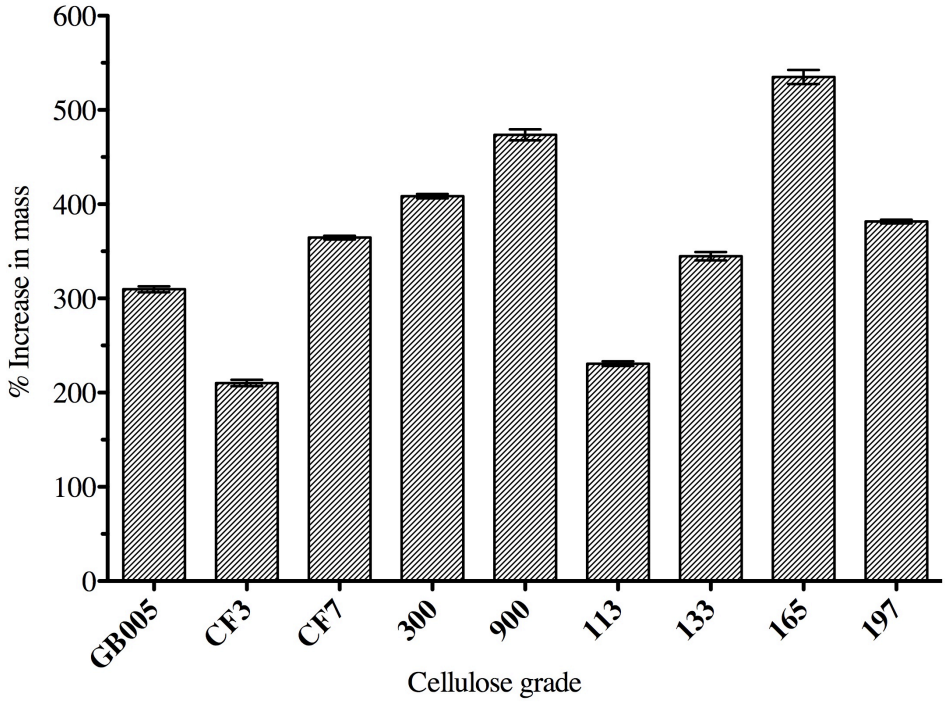

Figure 3. Maximum saline absorption by cellulose pads. The absorption capacities in percent increase in mass of nine cellulose materials with saline diluted to 50 mM sodium chloride are shown. Grade 165 had the greatest percent increase in mass following immersion in saline solution for 6 hours. Mean values ± standard error are given for n=6 samples. (1-way ANOVA, p<.0001)

Absorption tests were also performed with grade 165 cellulose pads using de-ionized water, 1x DPBS, and saline solutions of 20 mM, 50 mM, and 80 mM sodium chloride. These experiments revealed variation in absorption capacity due to ion concentration with statistical significance during short-term immersion (10 seconds to 90 seconds), but not when the duration of saline immersion exceeded 10 minutes. The distribution of absorption capacities for grade 165 cellulose pads following short-term immersion for 10 to 90 seconds is shown below in Figure 4. Differences were found to be significant using the nonparametric Kruskal-Wallis test (p<.0001). Previous statistical analysis showed that absorption capacity did not vary based on immersion time for the short-term, 10 to 90 seconds (p=.1584).

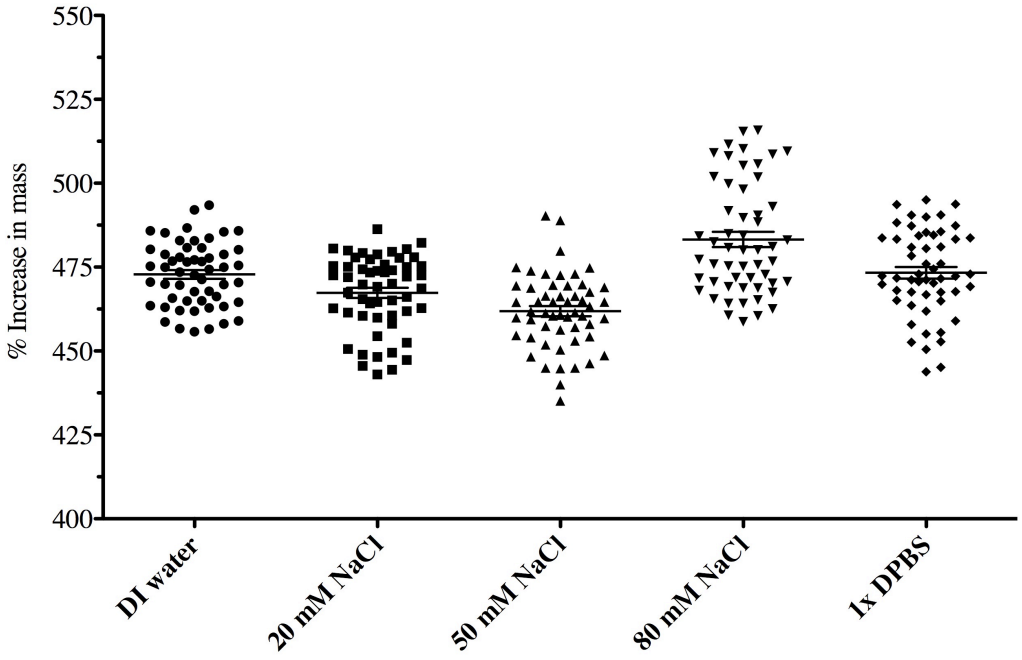

Figure 4. Variation in absorptive capacity due to saline concentration. The absorptive capacities in percent increase in mass collected over short-term absorption (10-90 s) are given for Grade 165 cellulose with de-ionized water and four saline concentrations (1xDPBS and DPBS diluted to 20 mM, 50 mM, and 80 mM sodium chloride). Mean values ± standard error are given for n=54 samples. Differences in absorption between these groups are significant (Kruskal-Wallis, $p<.0001$). Statistical significance is lost when the 80 mM NaCl group is excluded at each of the different immersion times (Kruskal-Wallis, $p>.05$).

Additional figures showing the mean absorption capacity of Pall grade 165 cellulose pads following immersion for 10 seconds to 90 seconds and for 10 minutes to 90 minutes can be found in Appendix A.

3.3 Moisture Vapor Transmission

A second material property that was considered was the moisture vapor transmission rate (MVTR) of the absorbent cellulose pads. The MVTR describes the ability for water vapor to pass through a material. The absorbent layer of the skin patch must efficiently transfer water vapor from the surface of the skin to prevent moisture accumulation from occluding sweat glands, while a patch cover must prevent excess evaporation to obtain an accurate measurement of sweat losses. The rate of evaporation of water from each grade of absorbent cellulose was studied by tracking the change in mass over a 12-hour period of samples saturated in saline solution diluted to 50 mM sodium chloride. The MVTR in grams per hour over a 6.25 cm^2 sample area was taken as the slope of the linear region of the graph showing change in mass over time. The MVTR of the nine grades of absorbent cellulose are compared in Figure 5. All evaporation experiments were performed in an environment of 24.6 ± 1.8°C and 22 ± 3% relative humidity.

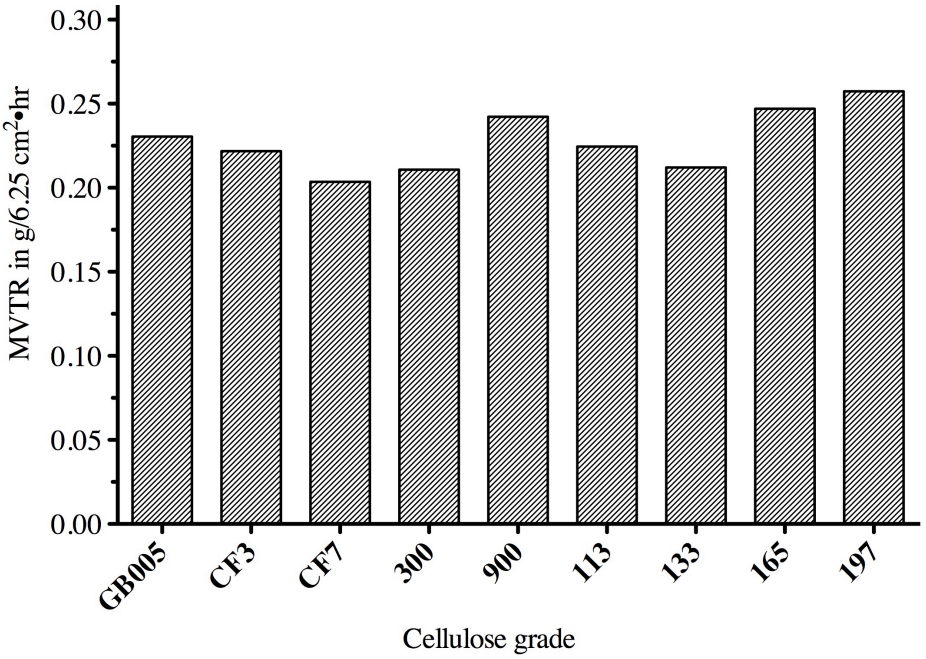

Figure 5. Moisture vapor transmission rates of absorbent cellulose sheets. The rates of moisture vapor transmission for each of the nine grades of absorbent cellulose were determined from cellulose samples saturated in saline solution diluted to 50 mM sodium chloride. The mass of each sample was tracked over a 12-hour period of evaporation, and the MVTR was taken as the slope of the linear region of the graph of change in mass over time.

The affect of ion content on the moisture vapor transmission through absorbent cellulose was also considered. The evaporation profiles of Pall grade 165 absorbent pads saturated with de-ionized water and saline solution diluted to 20 mM, 50 mM, and 80 mM sodium chloride were observed and the MVTR were calculated from the slope of the linear region of the curve. Variation in the mean MVTR (± standard error) due to saline concentration are shown in Figure 6, below. Differences in MVTR between the different saline solutions and de-ionized water are not significant (1-way ANOVA, p=.1531).

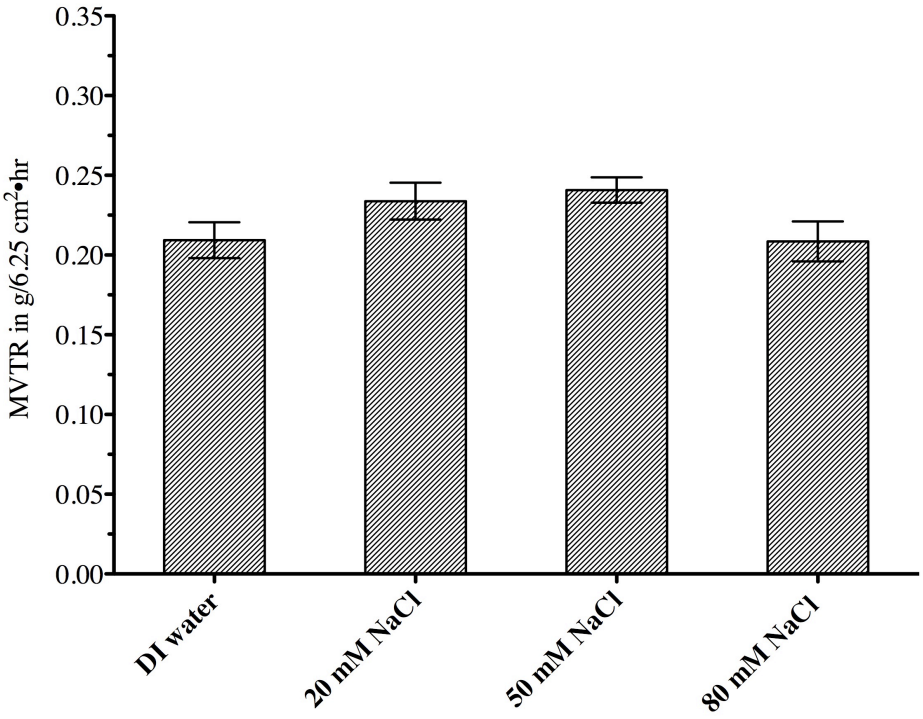

Figure 6. Moisture vapor transmission rates with various saline concentrations. The rates of moisture vapor transmission through grade 165 cellulose from Pall Corporation with de-ionized water and three different saline concentrations are shown as the mean ± standard error for three trials. The change in mass of each sample was tracked over 12 hours, and the MVTR was taken as the slope of the linear region of the graph of change in mass over time. Differences in MVTR between each of the solutions did not reach statistical significance (1-way ANOVA, p=.1531).

The proposed sweat patch design includes an adhesive film that holds the absorbent material on the surface of the skin. The rate of moisture transmission through this film, the 3M™

Tegaderm™ Holding Power (HP) transparent film dressing, measured and compared to the MVTR of grade 165 absorbent cellulose alone. The mean rates of moisture vapor transmission for cellulose alone (no Tegaderm™) and the skin patch consisting of cellulose sealed under a Tegaderm™ layer (with Tegaderm™) are compared in Figure 7. The MVTR of grade 165 cellulose (.244±.007 g/6.25cm^2•hr) was significantly reduced by the presence of the Tegaderm™ transparent film dressing (.034±.002 g/6.25cm^2•hr).

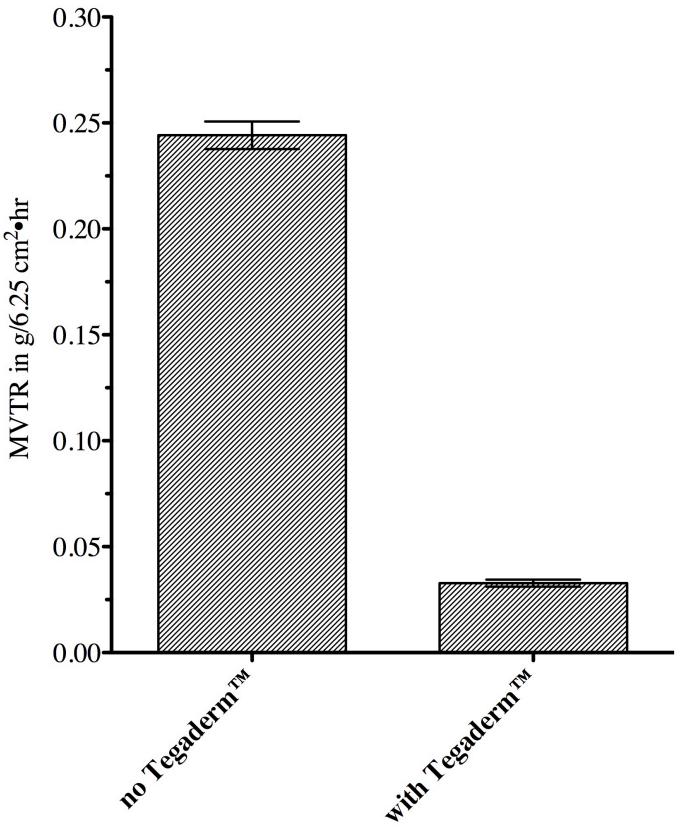

Figure 7. Reduction in MVTR with a Tegaderm™ film cover. The rates of moisture vapor transmission through Pall grade 165 cellulose alone (no Tegaderm™) and grade 165 cellulose with a transparent Tegaderm™ adhesive film cover are given as the mean ± standard error of 4 trials. The sample mass was tracked over a 12-hour period of evaporation (no Tegaderm™) or a 48-hour period of evaporation (with Tegaderm™), and the MVTR was taken as the slope of the linear region of the graph of change in mass over time. The MVTR was significantly reduced by the presence of the Tegaderm™ cover, MVTR=.033±.002 g/6.25cm^2•hr, versus cellulose alone, MVTR=.244±.007 g/6.25cm^2•hr (2-tailed t-test, p<.0001).

3.4 Images of Skin Patch Materials

Scanning electron microscope (SEM) images were taken of the skin patch materials to reveal the microstructure of the absorbent cellulose and to estimate the pore size of the Tegaderm™ transparent film dressing. The pore size of the Tegaderm™ film could not be determined using the minimum resolution of the microscope, approximately 1 μm. Samples of grade 165 absorbent pads from Pall Corporation were imaged to compare the cellulose structure following treatment in ethanol, absorption of de-ionized water, and absorption of saline solution diluted to 80 mM sodium chloride with an untreated sample. Images showing the nonwoven organization of the four samples are provided in Figure 8. Additional images at a greater magnification to show the structure of the individual fibers are presented in Figure 9. The cellulose fibers are approximately 10 μm in diameter with a roughened surface morphology. An additional SEM image showing the smooth structure of the Tegaderm™ film can be found in Appendix B.

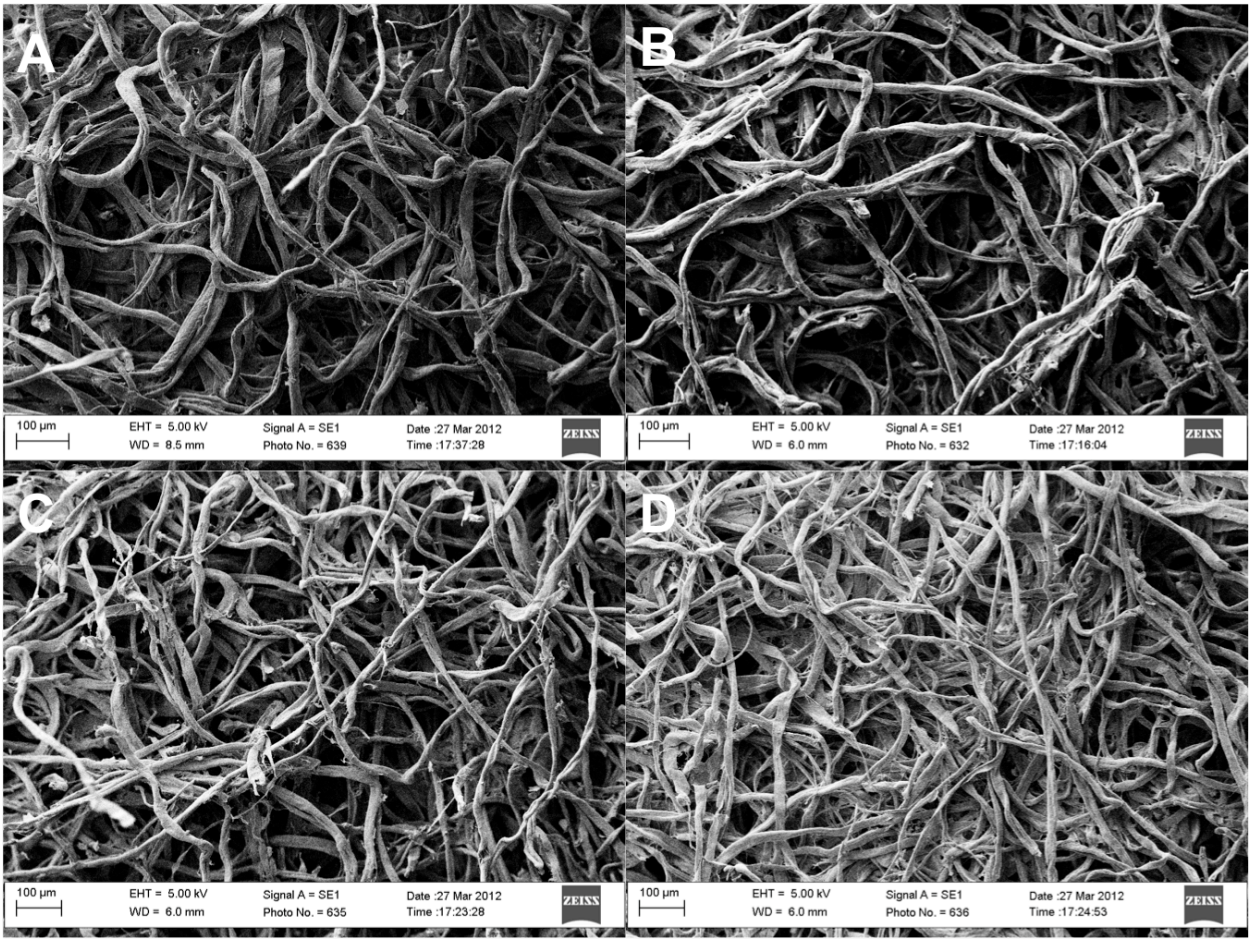

Figure 8. SEM images of absorbent cellulose. High-resolution images of Pall grade 165 cellulose pads reveal a porous, non-uniform fiber network microstructure. The images above represent different cellulose samples A) untreated, B) soaked in ethanol and dried at 60°C, C) soaked in ethanol, dried, and immersed in saline diluted to 80 mM sodium chloride, and D) soaked in ethanol, dried, and immersed in de-ionized water. No apparent differences in microstructure were noted.

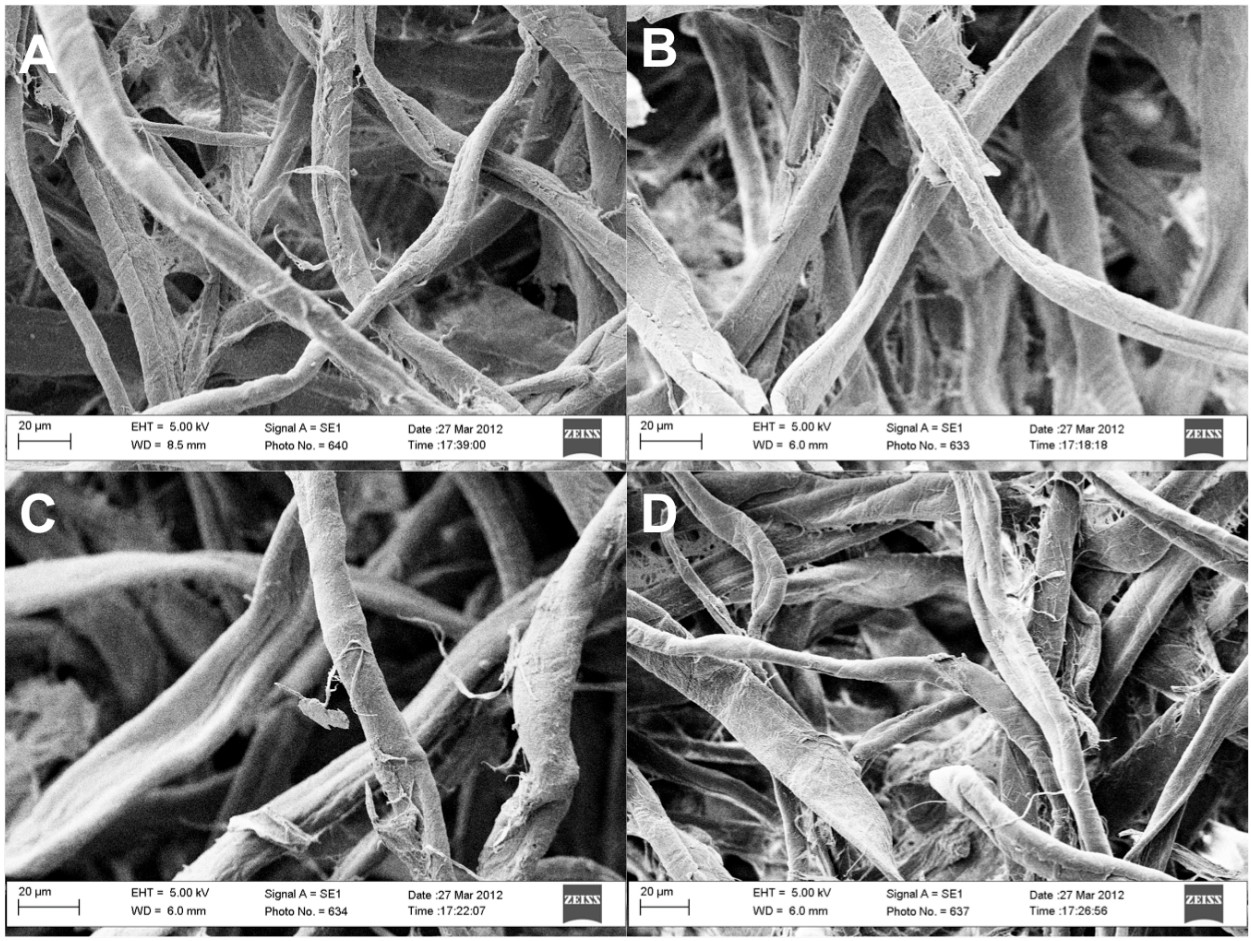

Figure 9. SEM images of cellulose fibers. The surface structure of individual cellulose fibers in grade 165 absorbent pads are shown. Each sample was exposed to a different treatment, where A) was untreated, B) was soaked in ethanol and dried at 60°C, C) was soaked in ethanol, dried, and immersed in DPBS solution diluted to 80 mM sodium chloride, and D) was soaked in ethanol, dried, and immersed in de-ionized water.

3.5 Radio Frequency Sensor Detection of Saline Solutions

Changes in the impedance spectrum of a commercially available RFID tag in contact with the skin patch were observed for different fluid volumes and ion contents. Analyzed variables included center frequency, bandwidth, quality (Q) factor, and reflective power losses. All trends described below were observed over two experimental trials.

Center frequency

Radio frequency (RF) measurements revealed distinct changes in the center frequency of the resonance peak due to the volume of solution absorbed by the cellulose layer. The center frequency decreased as the volume of saline or de-ionized water within the patch increased up to 4.5 mL. A graph displaying the shift in center frequency from the dry condition using de-ionized water and the average shift across the thirteen conductive saline solutions is shown in Figure 10. Differences in center frequency shift due to volume of solution were statistically significant in a one-way ANOVA ($p<.0001$). Detection of volume in the skin patch was most sensitive with volumes under 1 mL, shifting about 100 kHz per .25 mL. At volumes over 2 mL, center frequency shifted about 25 kHz per .25 mL of saline added.

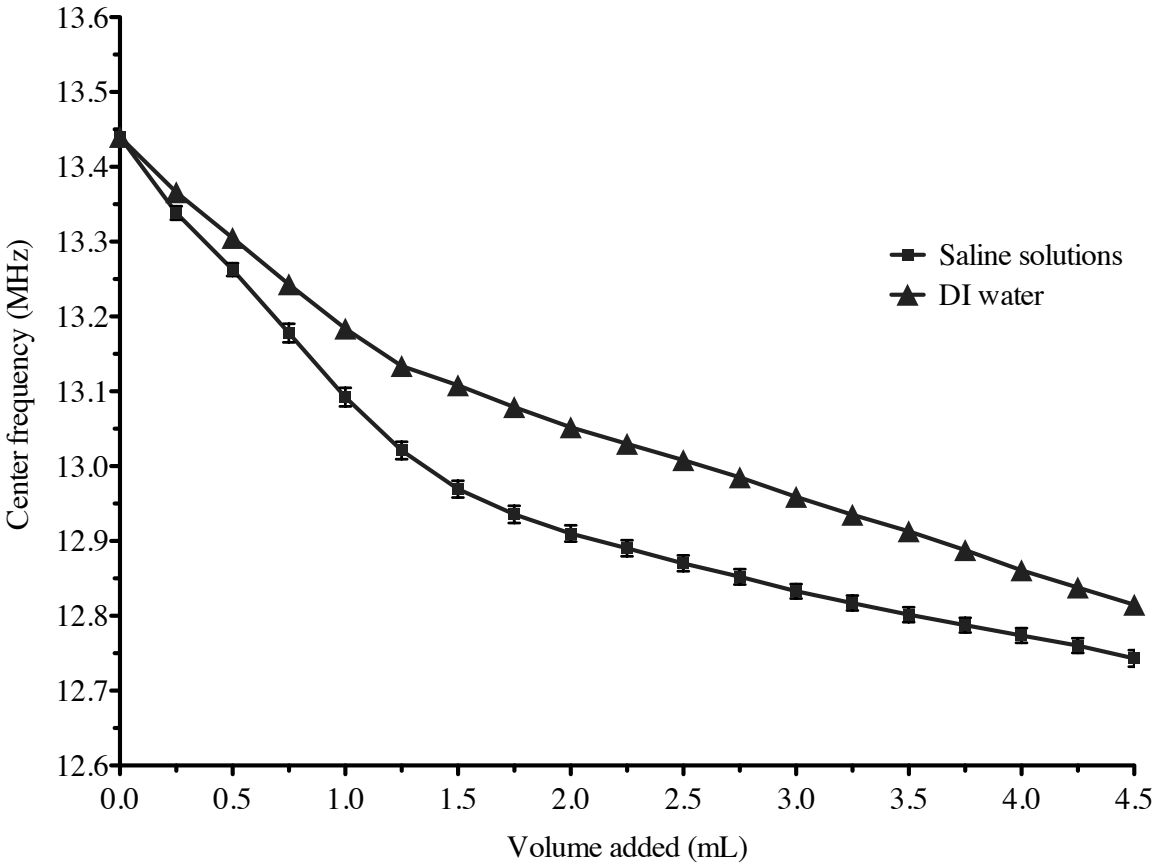

Figure 10. Decrease in center frequency with saline absorption. Center frequency of the resonance peak decreased with each addition of fluid (.25 mL) on the skin patch. The average center frequency for the thirteen conductive saline solutions (20 to 80 mM sodium chloride) is given as the mean ± SEM. The observed shift in frequency using de-ionized water is shown for comparison. Observed changes in center frequency due to volume of solution reached statistical significance in a one-way ANOVA ($p<.0001$).

The ability to detect changes in ion concentration of the fluid absorbed by the skin patch was also of interest. When analyzed independently, the center frequency did not vary due to ion content. The average center frequency across volumes of solution up to 4.5 mL for each of the thirteen diluted saline solutions and de-ionized water is shown below in Figure 11. Differences in center frequency between solutions were not significant based on a one-way ANOVA, $p=.8135$.

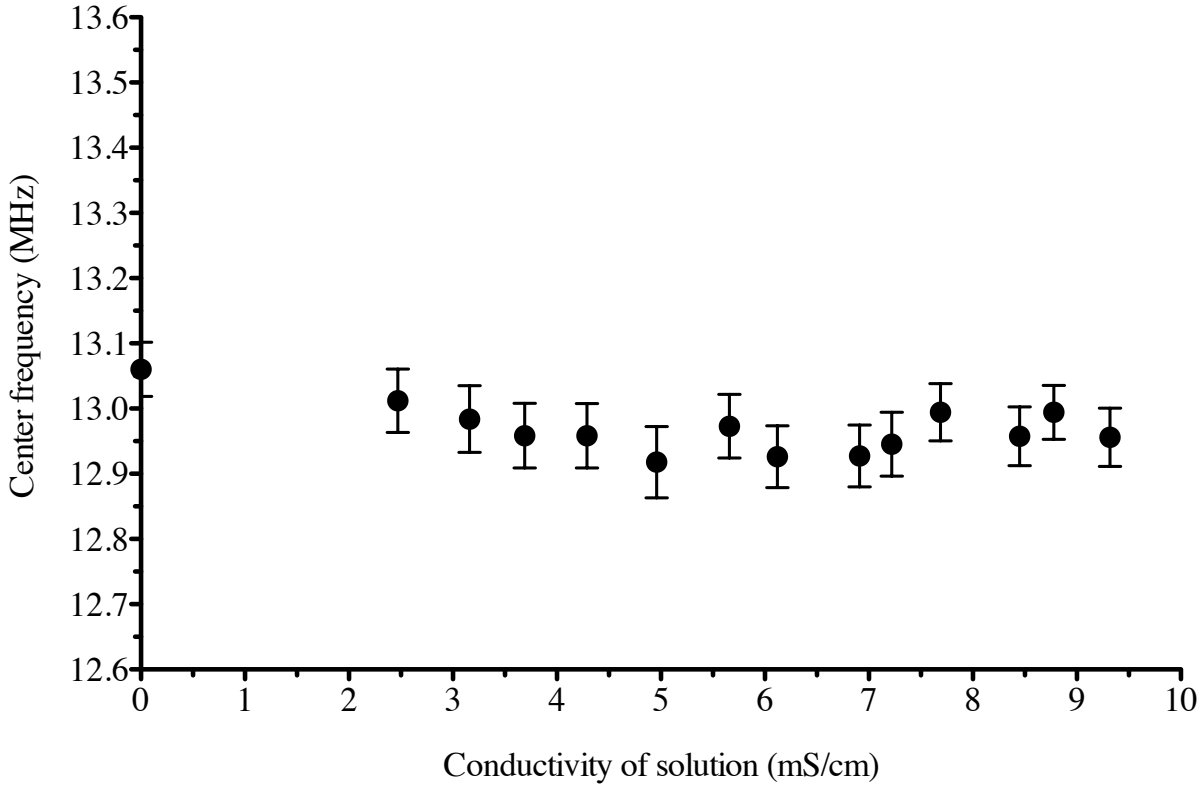

Figure 11. Average center frequency for saline solutions. Center frequency values were averaged for total solution volumes from 0 to 4.5 mL. The mean observed shift in center frequency ± SEM is displayed above. Differences due to ion content are not significant (one-way ANOVA, p=.8135).

An additional graph showing the shift in center frequency for each of the thirteen diluted saline solutions and de-ionized water can found in Appendix C, Figure 1C. Analysis by a two-way ANOVA revealed differences due to ion content and volume to be statistically significant ($p<.0001$). However, volume of solution contributed to much more of the total variation (95.39%) than ion content (3.23%).

Bandwidth

Changes in the bandwidth of the reflective losses were also observed as the volume of saline in the sweat patch increased. A graph showing how the bandwidth changed for each of the saline solutions and de-ionized water as volume increased is shown in Figure 12. Observed

changes in bandwidth between volumes of solution increasing in .25 mL aliquots are significant based on analysis by a one-way ANOVA ($p<.0001$).

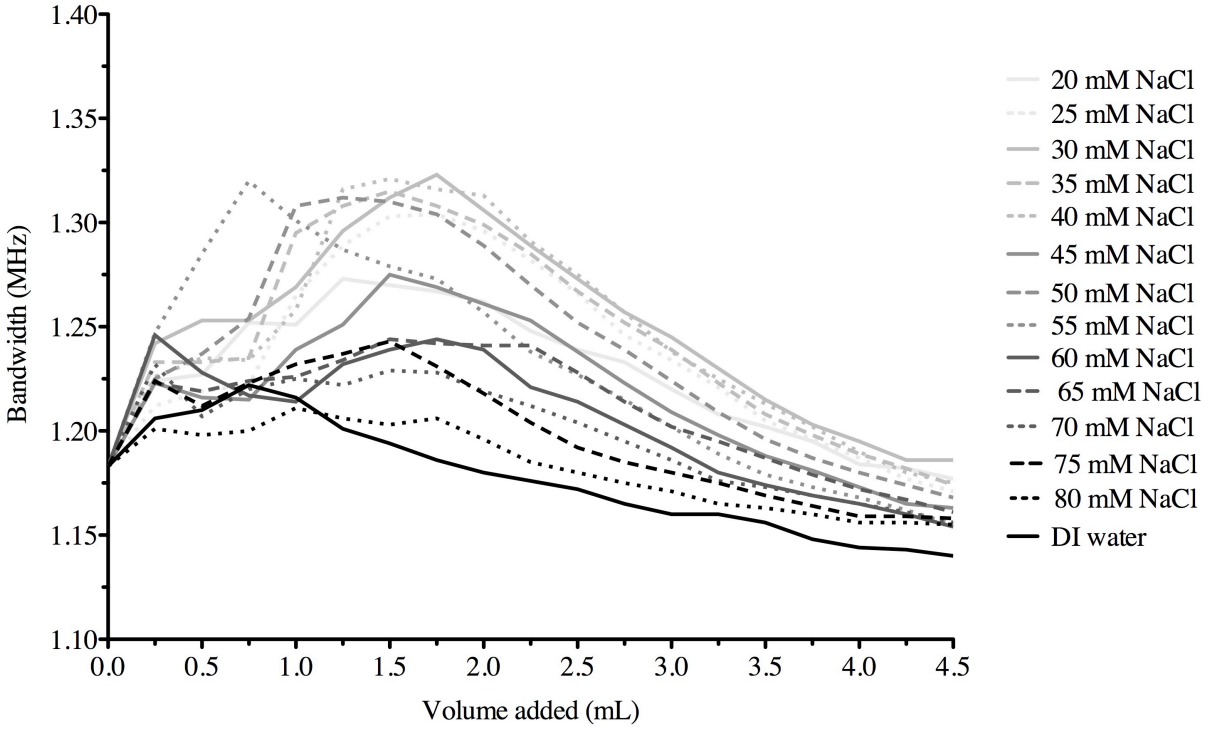

Figure 12. Change in bandwidth with saline absorption. The bandwidth of the resonance peak changed with the addition of fluid in the absorptive layer of the skin patch. Changes in bandwidth for each of the thirteen dilute saline solutions and de-ionized water are shown. Variation in bandwidth due to volume of solution reached statistical significance in a one-way ANOVA ($p<.0001$).

Bandwidth was averaged across all solution volumes (up to 4.5 mL) and compared in order to examine changes due to ion content alone. Changes in bandwidth due to the total conductivity of each of the experimental solutions are shown in Figure 13, below. Although differences due to conductivity reached statistical significance in a one-way ANOVA ($p<.0001$), no consistent trend could be discerned in the signal bandwidth for increasing solution conductivity.

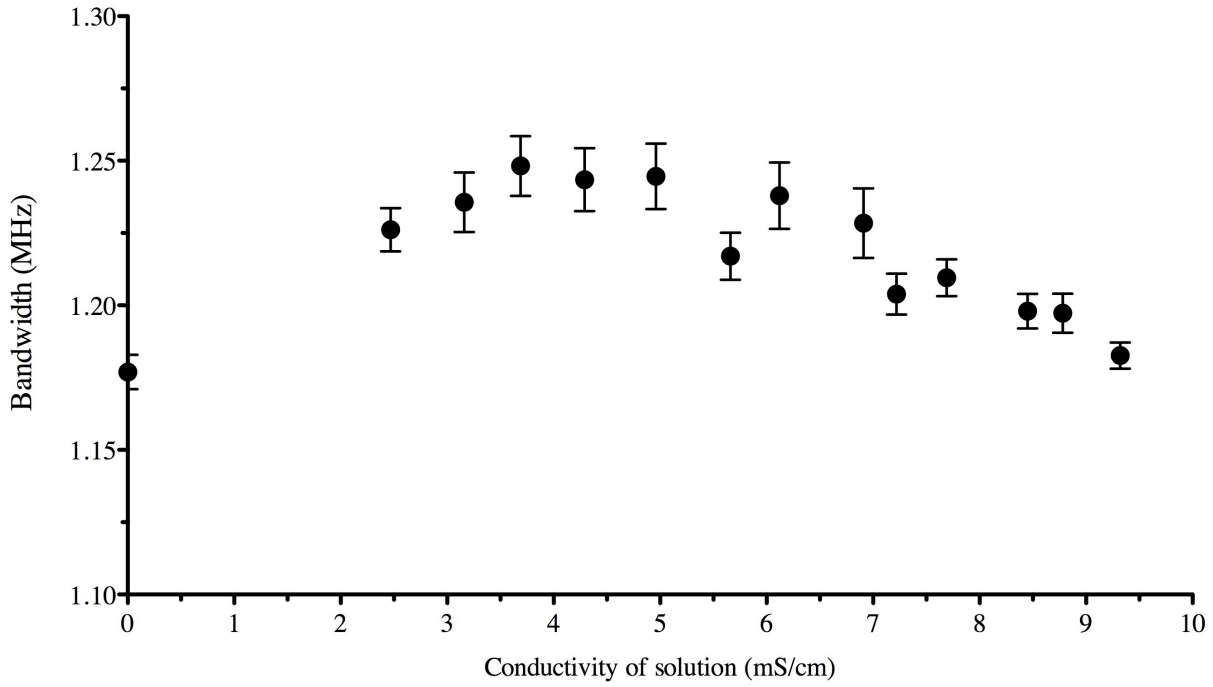

Figure 13. Average bandwidth for saline solutions. The bandwidths for total solution volumes from 0 to 4.5 mL were averaged for each of the thirteen saline solutions and de-ionized water. The mean bandwidth ± SEM is shown. Differences due to ion content are significant (one-way ANOVA, $p<.0001$).

The Q factor and the magnitude of the reflected power were also recorded and analyzed. Changes in the Q factor, calculated as the center frequency divided by the bandwidth, were graphed to reveal similar changes due to volume and conductivity of solution in the skin patch. These graphs can be found in Appendix C, Figures 2C and 3C, respectively. Differences in the Q factor due to both volume of solution and solution conductivity were statistically significant in a one-way ANOVA ($p<.0001$).

The magnitude of the reflected power losses varied slightly with volume and conductivity of solution within the skin patch. These trends are shown in Appendix C, Figures 4C and 5C. Again, observed variations between the reflective losses and volume and conductivity of solution reached statistical significance (ANOVA, $p<.0001$).

Chapter 4: Discussion

4.1 Skin Patch Design and Selection of Materials

The materials used for sweat collection on the surface of the skin were an important consideration for the proposed sweat indicator. The patch must absorb sweat faster than the rate of secretion in order to avoid occlusion of the sweat glands or reabsorption of the sweat by the stratum corneum. If sweat absorption by the patch is rate limiting then the buildup of excess moisture over the glands could lead to a decrease in the local sweat rate, which will underestimate whole body sweat losses (Collins 1962). The presence of a dilute aqueous solution against the skin can also lead to electrolyte leaching from the stratum corneum, resulting in an overestimation of sweat electrolyte concentrations (Weschler 2008). Therefore, the patch must collect and lock moisture away from the skin to avoid occlusion of sweat glands and electrolyte leaching from the stratum corneum. In addition, the patch absorption capacity must match maximum sweat rates over a period of time, so that all sweat secreted over a given area can be analyzed. Endurance athletes, such as marathon runners, may need to wear a single patch for upwards of five hours. For this project, a skin patch was designed to be worn for up to 3 hours of physical activity at maximum expected sweat rates.

The preliminary skin patch design included a thin absorbent layer to be held under an adhesive cover and RFID tag, as shown below in Figure 1. Two layers of a thin film adhesive were used: one to hold the skin patch on the skin, and a second to act as a sensing layer on the RFID tag. The materials selected for use within the patch must be non-irritating to the skin, as even minor irritation caused by the skin patch could be a distraction for the athlete. Additionally, the patch must be flexible to conform to the surface of the skin and should not be stiff or bulky.

The final collection device must be a thin patch that can be worn comfortably during physical activity.

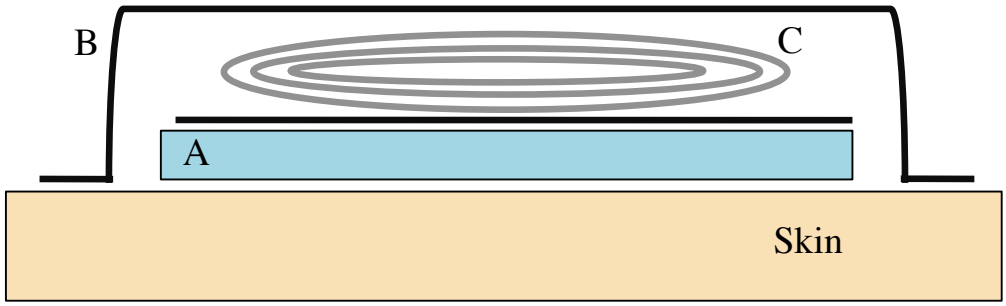

Figure 1. Sweat patch design. An absorbent layer (A) will rapidly absorb and hold sweat collected from the surface of the skin. A transparent cover (B) will adhere the patch to the skin and also provide a protective layer between the antenna coil (C) and the absorbent layer (A) for RF measurements.

In this design, the size of the patch was determined from the dimensions of a commercially available 13.56 MHz RFID tag. A 5 cm by 5 cm absorbent layer would match the approximate size of the tag, so that all collected sweat would be held in the vicinity of the coil for RF detection. The materials that were selected to test in a preliminary sweat patch design were cellulose for the absorbent layer and a transparent film wound dressing for the cover. These materials are non-irritating, inexpensive, as well as thin and flexible. Various options were also considered for an appropriate fluid to use for material and radio frequency testing. Diluted saline solution was ultimately chosen as an optimal fluid for these experiments because it is inexpensive, readily available, and similar in content to human sweat.

Absorptive layer

Cellulose is chosen as an ideal material for the absorptive layer of the skin patch. Structurally, cellulose is a carbohydrate that is comprised of repeating glucose molecules linked by beta acetal linkages. As shown in Figure 2, a number of hydroxyl groups surround the carbon chain. In aqueous solutions, these hydroxyl groups become negatively charged and attract water molecules and ions, allowing cellulose to absorb large amounts of water. Owing to its

hydrophilicity, cellulose should be able to hold large amounts of water and sweat electrolytes tightly below the RF coil. In addition, cellulose is a naturally occurring and uncharged polymer that will not cause skin irritation. Nine grades of thin, nonwoven cellulose absorbent pads were obtained for absorption testing. A nonwoven structure is made from various fibers thermally or chemically bound together in a random web-like arrangement, whereas a woven structure is knit or weaved together from a continuous fiber. Nonwoven materials will typically have a larger exposed surface area and smaller pore size than woven materials (Deitzel 2000). The selected cellulose pads range in thickness from .3 to 2.6 mm with various reported pore sizes. The thinnest cellulose grade capable of rapid absorption of adequate sweat volumes in laboratory experiments will be chosen for use within the skin patch.

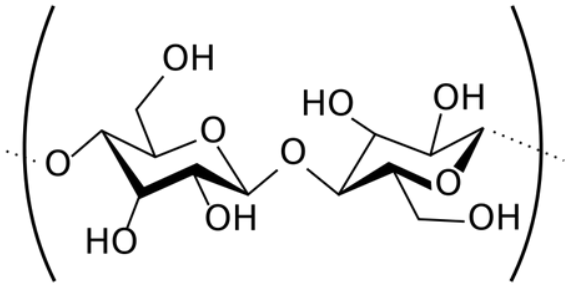

Figure 2. Cellulose structure. Repeating glucose monomers connected by beta acetal linkages make up the cellulose polymer. The presence of the hydroxyl groups surrounding the carbon chain make this a hydrophilic molecule. (Photo: Helmenstine 2012)

Adhesive film

Two protective film layers will be used to hold the absorbent cellulose on the surface of the skin and to act as a sensing layer between the RFID coil and the sweat patch contents. The outer cover must strongly adhere to the skin, especially under high humidity, as the patch will be worn for upwards of 3 hours during physical activity. It is important that the patch is held firmly in place without any shifting during movement so that an accurate measurement of sweat patch contents can be recorded. The cover must also be completely impermeable to fluids and particles

entering from outside the patch. Substances such as sweat, water, and dirt present in the exterior environment must not permeate the patch cover, so that only sweat collected over a specific skin area is present in the absorbent layer. From the interior, the patch should be breathable to prevent the excess buildup of moisture against the skin, which could occlude the sweat glands and decrease secretion (Collins 1962). An additional film layer will aid in radio frequency detection of the sweat patch contents by serving as a protective sensing layer between the coil and the absorbent layer. If the antenna coil were held directly in contact with a conductive fluid, such as the sweat, there would likely be significant losses in sensor resonance. The presence of a thin film layer adhered to the coil should prevent early saturation of the RF signal to allow for more sensitive detection of patch contents. A transparent wound dressing, Tegaderm™ sold by 3M™, was selected as an ideal material to hold the patch on the surface of the skin and to provide a sensing layer on the RFID coil. As an adhesive wound dressing, this material was designed as a breathable layer to prevent excess moisture accumulation while blocking the entry of foreign substances to the injury site. Experiments to test the rate of moisture transmission through the skin patch and the sensitivity of RF detection of collected sweat will be used to determine whether Tegaderm™ was an appropriate choice for the adhesive film.

Saline "sweat" solution

Skin patch material tests needed to be performed with a fluid that is similar to the contents of sweat. Human sweat, artificial sweat, saline, and water were all potential fluids for use in material tests. Use of human sweat would provide the most relevant data for the device application, but the collection of suitable quantities would be time consuming, expensive, and require strict isolation precautions and storage guidelines. Artificial sweat is sometimes used as an alternative to human sweat, and is even described in an ISO Standard (ISO 3160-2). A typical

formulation includes sodium chloride, ammonium chloride, acetic acid, lactic acid, and sodium hydroxide to a pH of 4.7. While adjusted to match the pH of sweat, artificial sweat lacks some key electrolytes found in the sweat: potassium, calcium, and magnesium. In addition, lactic acid is expensive and is such a minor sweat constituent that it is unlikely to have any significant effect on fluid wicking and absorption into the patch. The simplest and least expensive choice would be to use water for material testing, as sweat is 99% water. When considering the material properties that would be tested, however, the absorption capacity and rate of fluid uptake of cellulose may be affected by the interaction of charged species in aqueous solution. Therefore, diluted Dulbecco's phosphate buffered saline (DPBS) was chosen as an appropriate fluid for all material and radio frequency testing. DPBS is readily available, relatively inexpensive, and because it is isotonic to extracellular fluid, it contains all major electrolyte found in the sweat.

Because the sweat is hypotonic to the extracellular fluid, saline solution were diluted to ion concentrations between 20 mM and 80 mM of sodium. This is the normal physiological range for sweat sodium, the most abundant ion found in human sweat. A total of thirteen diluted solutions were prepared, each differing in total ion content by 10.3 mOsm/L and in sodium chloride content by 5 mM. These solutions were used for material tests to study the absorption and fluid transmission properties of the skin patch as well as for radio frequency measurements to detect variations in solution volume and conductivity within the skin patch.

4.2 Properties of the Skin Patch Materials

With a preliminary skin patch design (Figure 1), the first aim was to test the material properties of the absorbent cellulose pads and Tegaderm™ . Experiments were designed to test whether the proposed patch design would be a good local sweat collector for subsequent radio frequency quantification. The first parameter to be examined experimentally was cellulose

absorption. Two factors were considered: the total amount of saline absorbed and the percent by mass of fluid that each cellulose grade could absorb. From existing data on regional collection (see Chapter 2, Figure 6), the sweat patch would need to collect sweat volumes of up to .3262 mL/cm^2 per hour on the forehead, .0744 mL/cm^2 per hour on the chest, .0487 mL/cm^2 per hour on the chest, .2094 mL/cm^2 per hour on the lower back, and .0607 mL/cm^2 per hour on the thigh at high exercise intensities (Smith 2011). The thigh was selected as the most optimal patch location because it has been previously reported that sweat collected here strongly correlates to total body sodium and potassium losses as well as to whole body sweat volume losses (Baker 2009, Patterson 2000, Smith 2011). Over a patch area of 25 cm^2 on the thigh, sweat volumes of up to 1.5175 mL per hour could be expected. It is important to consider that this is the maximum sweat rate observed in a single individual over 30 minutes of high intensity running, and that the mean sweat rate observed by Smith and colleagues at the thigh was about half this volume, at .6775 mL per hour. As sweat rate varies so widely between individuals, however, it will be crucial for the sweat patch to have an absorption capacity to match that of heavy sweaters. To meet these demands, the cellulose layer must be able to hold at least 4.5 mL, which would allow the patch to be worn for about three hours continuously at these heavy sweat rates.

The absorption capacities of nine grades of cellulose pads were determined experimentally, and it was found that four materials could hold at least 4.5 mL of saline when immersed for 10 seconds. The next parameter that was considered was the cellulose thickness. When the absorption capacities were expressed in terms of percent increase in mass, grade 165 absorbent cellulose from Pall Corporation was able to absorb a significantly greater percentage of its mass than any of the other materials (534.98± 7.43%). With an average thickness of 1.8 mm, this material was the thinnest material of the four materials capable of absorbing at least 4.5

mL of solution. Grade 165 was the least bulky material that met the required absorption capacity of 4.5 mL and was therefore chosen as the optimal absorptive layer for sweat collection within the skin patch.

An additional property that was examined was the breathability of the skin patch materials. Specifically, the moisture vapor transmission rate (MVTR) was measured. The MVTR investigated here describes the rate at which water vapor can permeate through the absorbent cellulose or, as tested in a later experiment, through the absorbent cellulose and Tegaderm™ cover. Breathability was similar between the nine cellulose grades, ranging in MVTR from .2036 to .2574 g/6.25 cm^2•hr. Statistical significance cannot be determined because the rate of evaporation was only measured once for each cellulose grade. When converted to conventional units, these cellulose pads had an MVTR of 7818.24-9884.16 g/m^2•24 hrs. For comparison, the rate of transepidermal water loss for the average male at rest is ranges from about 200 to 4000 g/m^2•24 hrs, and during high intensity exercise these values increase to 1200 to 1440 g/m^2•24 hrs (Guo 2011). The rate of vapor transmission through the cellulose pads is much high than the rate of water transmission through the skin. This is ideal because the cellulose should provide a breathable layer to transmit moisture through the pad and away from the skin, preventing the occlusion of sweat glands.

The rate of moisture transmission through grade 165 absorbent cellulose covered by a layer of Tegaderm™ HP was also studied. The presence of the Tegaderm™ reduced the MVTR from .244±.007 g/6.25cm^2•hr , with grade 165 cellulose alone, to .033±.002 g/6.25cm^2•hr. At this rate, the sweat patch could lose up to .132 mL of sweat each hour. This would lead to a total sweat loss of .396 mL over 3 hours of wear, or 8.8% of the total cellulose absorption capacity. These losses, however, are calculated from a patch that is completely saturated with solution.

During actual wear, sweat contents within the patch will be increasing over a period of 3 hours and thus there will be less of a gradient for fluid transmission through the patch.

The transmission of moisture through a material occurs due to differences in vapor pressure, or relative humidity. Particles will move from the side with higher relative humidity to a lower humidity (Wu 2007). Because the vapor pressure of water increases steadily with temperature, the temperature of the local environment has a substantial effect on the rate of vapor transmission. These experiments performed here on moisture transmission through the skin patch materials are limited in that all rates of evaporation were measured at 24.6 ± 1.8°C and 22 ± 3% relative humidity. The average skin temperature during exercise ranges from 29°C to 36°C depending on intensity (Cheuvront 2007), while humidity levels will vary due to the ambient conditions and clothing worn. Previous studies have demonstrated that the rate of moisture transmission through various film dressings increases with temperature and decreases with humidity of the local environment (Yu-Shuang 2009). With this in mind, elevated temperature of the skin should speed the transmission of moisture through the absorbent layer of the patch in contact with the stratum corneum. This would serve to more effectively transport moisture away from the sweat pores, but could also increase the total evaporative losses of the patch. The effect of humidity on the rate of moisture transmission through the patch will depend on the difference in humidity interior and exterior to the patch itself. On a humid day, or if the patch is worn under fitted clothing, moisture transmission will be slowed because there will less of a gradient for moisture to evaporate through the patch. Under dry or cool conditions, however, a higher rate of moisture transmission through the patch is expected. The experiments performed here allow for a rough estimation of the expected evaporative sweat losses from the skin patch, but further work

should aim to measure the MVTR of the skin patch under conditions that more closely match those on the skin of an exercising athlete.

Through additional experiments using grade 165 absorbent pads, the effects of ion content on cellulose absorption were studied. The same parameters of absorption capacity and the rate of moisture transmission were measured using de-ionized water and saline solutions containing 20 mM, 50 mM, and 80 mM sodium chloride. For all previous absorption measurements, saline solution diluted to 50 mM sodium chloride, the average sodium content of human sweat (20-80 mM), was used. In terms of moisture evaporation, it was found that the MVTR through cellulose was not affected by variation in ion concentrations up to 80 mM sodium chloride, or a total ion content165 mOsm/L. The grade 165 cellulose pads have a nominal micron rating 25 μm, meaning that the majority of particles measuring 25 μm can permeate this material (Pall Corp.). This pore size is orders of magnitude larger than the expected size of ions in aqueous saline solution, and therefore the presence of ions should not have a significant effect of the transmission of water vapor through the material.

The affect of ion content on cellulose absorption capacity was also studied. It was found that the absorption capacity of cellulose was statistically different between these four saline concentrations and undiluted saline solution when analyzing cellulose absorption after short-term immersion, for 10 to 90 seconds. The non-parametric Kruskal-Wallis test was used here because one of the experimental groups, 80 mM sodium chloride, did not follow a Gaussian distribution. Although this difference was significant, statistical significance is lost (ANOVA, $p>.05$) when the 80 mM group is excluded from analysis at each of the individual immersion times from 10 seconds up to 6 hours. If ion content did have an effect on fluid absorption by cellulose, a trend should be apparent between each of the five solutions. Instead, the results indicate that a single

group, for 80 mM saline absorption, may have produced the highest mean percent increase in mass because of its non-Gaussian distribution. The potential affect of saline solution on cellulose absorption should be the topic of further research. For the purpose of this project, any variations on cellulose absorption due to ion content within a physiological range were considered to be slight, and these differences were not expected to affect the overall collection and analysis of sweat within the skin patch.

In preparation for radio frequency measurements within the skin patch, the effect of fluid absorption on the resistivity of the cellulose pads was studied. Cellulose alone is an insulator, meaning that it is highly resistive to the flow of an electrical current. Dry cotton fabric, which is mostly fibrous cellulose, has a reported electrical resistivity of 3.0×10^8 MΩ•m (Lekpittaya 2004). Saline solutions, however, are highly conductive due to the presence of ions to transmit an electrical current. The conductivities of the thirteen test solutions were measured, and the resistivity of these solutions varied from 4.05 Ω•m (20 mM sodium chloride) to .609 Ω•m (80 mM sodium chloride). It was expected that the resistivity of the cellulose pads would decrease sharply with the absorption of saline solution. One previous study investigated the changes in resistivity of knit cotton due to saline absorption and found that the absorption of saline up to 4% NaCl content caused a rapid decline in the material resistivity to the order of a few kΩ (Wang 2009). The resistivity of the cotton leveled off and did not continue to decrease with ion concentrations over 4%. A solution of 4% sodium chloride by mass is equivalent to 684 mM sodium chloride or 1368 mOsm/L, far more concentrated that the saline solutions used in these experiments, with concentrations ranging from 41 to 165 mOsm/L. Within this range of saline concentrations, the measured resistivity of cellulose should decrease with increasing ion content.

The experimental setup using a four-probe technique was unsuccessful in determining the electrical resistivity of absorbent cellulose following saline absorption. When applying a constant voltage across the sample, a steady measurement of the voltage drop between the two inner leads could not be recorded. The voltmeter reading changed continuously between voltage measurements varying by orders of magnitude from a few microvolts to tens of volts, and no consistent pattern could be observed between trials using different cellulose samples. When the voltage supply was increased to 20 volts, the cellulose sample developed a green-blue color at one point of lead contact as shown in Figure 3. This observation led to the assumption that electrolysis at the leads was interfering with the resistivity measurement. When the copper leads were placed in contact with the salt solution on the cellulose pad to close the circuit, oxidation of copper occurred at the anode by the following reaction:

$$Cu_{(s)} \rightarrow Cu^{2+}_{(aq)} + 2\ e^-$$

The production of copper (II) ions caused the green-blue color that was observed. It is likely that electrolysis led to an accumulation of ions at the wire contact points on the cellulose, preventing an accurate voltage readings in the resistivity measurements.

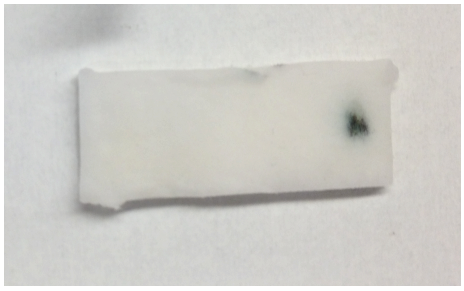

Figure 3. Electrolysis on absorbent cellulose. Electrolysis of copper at the anode resulted in a blue-green color on samples of the absorbent cellulose pads during resistivity measurements. Accurate measurements of cellulose resistivity after saline absorption could not be obtained using a DC voltage.

One way that electrolysis could be reduced is by using an alternating current. This would reduce the accumulation of ions because the polarity of the leads would be repeatedly switching. Measuring the resistivity over a range of frequencies could minimize the effect of electrolysis

even further. While the redesign of the four-point setup using an alternating current was beyond the scope of this project, future experiments to measure the resistivity of the absorbent pads would be beneficial in order to better understand the changes in cellulose properties that occur upon saline absorption.

4.3 Cellulose Structure

High resolution imaging by scanning electron microscopy (SEM) revealed a porous, non-uniform fiber network of grade 165 absorbent cellulose that is characteristic of nonwoven materials. From these images, the diameter of the cellulose fibers could be estimated at about 10 μm. Prior to all absorption experiments, cellulose samples were soaked in pure ethanol and dried overnight at 60°C. This procedure was used to ensure that all samples were completely clean and dry, providing a baseline to measure and compare absorption capacity between samples. One concern, however, was that ethanol treatment and exposure to heat may alter either the surface structure of the fibers or the overall organization of the fiber network. This hypothesis was rejected after SEM analysis failed to reveal any apparent structural differences between a sample that had been cleaned and dried and an untreated sample.

Similarly, imaging was performed to determine whether fluid absorption affected the fiber morphology or network organization of the absorbent cellulose pads, such as by dissolution of the fibers. In the process of SEM imaging, samples are subject to vacuum pressure and all moisture is vaporized. Therefore, the structure of hydrated cellulose samples could not be visualized using this imaging technique. However, any permanent changes induced on the cellulose pads from the absorption of fluid would still be observed. Previous work has reported the dissolution of nonwoven cellulose at temperatures over 70°C when soaked in non-aqueous ionic liquids (Swatloski 2002). Obvious changes were noted in the dissolved samples when

imaged using SEM, as the fibers appeared clumped together in an amorphous shape. It was postulated that this dissolution occurs by breaking of the hydrogen bond network between the glucose chains. The use of aqueous solvents inhibited this process, likely because the water molecules held the hydrogen bond network intact (Swatloski 2002). When the cellulose samples were imaged after immersion in de-ionized water or saline solution diluted to 80 mM sodium chloride, there were no apparent changes in fiber morphology or organization to indicate dissolution. Dissolution of the absorbent cellulose pads is not a concern for this application because the test solutions and human sweat contain large amounts of water that will hydrogen bond to the cellulose chains.

SEM imaging revealed that while the grade 165 cellulose does not contain uniform pores, gaps between neighboring fibers typically span at least 25 μm. This gap size is orders of magnitude larger than ionic compounds present in aqueous solutions, which are typically a few nanometers in size when ion-water interactions are considered (Marcus 1988). Gaps in the cellulose pads are also substantially larger than the size of proteins and amino acids, which are no larger than tens of nanometers. All constituents of the sweat, therefore, should pass freely into the cellulose pads during absorption. With the exception of dirt or debris that may be present on the surface of the skin, the cellulose is not expected to filter out any particles. Once absorbed, hydrogen and ionic bonding of the cellulose hydroxyl groups to water, ions, and polar amino acid side chains should hold sweat constituents in the absorbent layer.

The high MVTR of grade 165 absorbent cellulose pads, 9369 $g/m^2 \bullet 24$ hrs, is evidence of the ability of water vapor molecules to pass freely through the material. The addition of the Tegaderm™ layer effectively reduced the rate of vapor transmission to 1267 $g/m^2 \bullet 24$ hrs. SEM images of an unstretched Tegaderm™ sample were taken in order to estimate the pore size of this

material. These images, however, showed only a smooth surface morphology and failed to show the individual pores of the polyurethane film. This may be because the pore diameter of the unstretched film is too small to be seen with the minimum resolution of the microscope, in which case the pore size is estimated to be on the order of hundreds of nanometers or less. It is also possible that the pores could not be visualized because of the presence of inorganic filler molecules, such as calcium carbonate or titanium oxide. In a common processing technique, the filler molecule is dispersed over the film polymer and weakly adheres to the polymer matrix (Wu 2007). When stretched, such as during application of the film to the skin, the adhesion between the filler and polymer substrate is broken and micropores are formed. Therefore, it is likely that SEM images of a stretched Tegaderm™ sample would reveal a structure with small micropores consistent with prior MVTR measurements.

4.4 Demonstrated RFID Sensor Capabilities

The second aim of this project was to detect changes in the fluid content within the absorptive layer of the skin patch using a passive radio frequency identification sensor. Measurements were performed to detect the volume of solution in the patch, in order to estimate total sweat losses, and the solution conductivity, to estimate the amount of electrolytes lost in the sweat. Distinct changes due to the volume of fluid within the skin patch were observed, but no consistent changes in sensor impedance due to ion concentration within the physiological range of sweat could be detected.

In the experimental setup described in Chapter 5, a RFID tag operating at a frequency of 13.56 MHz was covered with a layer of unstretched Tegaderm™ film and inductively coupled with a sensing coil from a reader, a vector network analyzer. A 5 cm by 5 cm sample of grade 165 absorbent cellulose, equal in size to the RFID tag, was placed directly on top of the tag and

Tegaderm™ film. As fluid was added to the cellulose pad, the network analyzer measured the impedance spectrum of the tag in a S11 parameter measurement. The S11 parameter, or scattering parameter, is a measurement of power reflected from the tag back to the sensing coil on the reader. Four variables were recorded from the network analyzer for each measurement: the center frequency, bandwidth, quality (Q) factor, and reflected power (Figure 4).

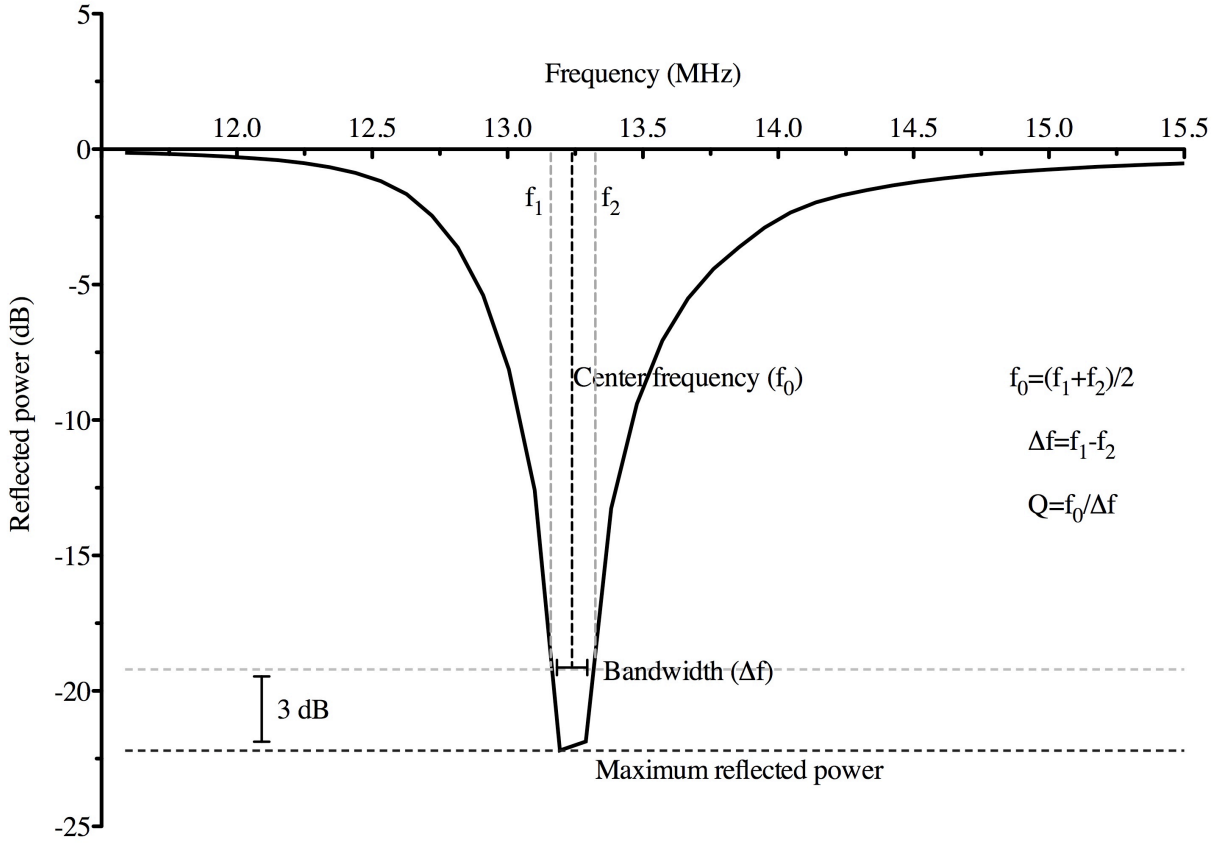

Figure 4. Magnitude plot of the S11 parameter. The center frequency, bandwidth, Q factor, and reflected power as recorded for each measurement are shown. These four variables characterize the impedance spectrum of the RFID tag for the radio frequency detection of fluid within the skin patch.

As illustrated in the figure, the maximum reflected power loss, in decibels, is taken as minimum point on the magnitude plot. The frequency at which reflected power is maximized is the minimum frequency. The center frequency and bandwidth are determined from the upper and

lower cut-off frequencies, or the frequencies at which the reflected power is at approximately one half its maximum value. The upper (f_2) and lower (f_1) cutoff frequencies are shown in Figure 4 at 3 dB from the maximum reflected power. The center frequency is calculated as the average of these two cutoff frequencies, while the bandwidth is calculated as the difference between these two frequencies. The Q factor describes the sharpness of the resonant peak, and is given as the ratio of the center frequency to the bandwidth.

Radio frequency measurements showed that the volume of saline within the sweat patch could be determined from the shift in center frequency. As volume increased from 0 to 4.5 mL, the center frequency decreased steadily. The center frequency decreased about 100 kHz per .25 mL of fluid for the first 1 mL of solution, and about 25 kHz per additional .25 mL of solution. This finding shows that the amount of fluid collected in the skin patch can be determined based on a single parameter, the change in center frequency from an initial baseline measurement.

This observed change in frequency can be explained by RF theory. The total impedance (Z) of the RFID tag is the sum of the resistive (R) and reactive (C, L) elements:

$$Z= R + j\omega C + 1/j\omega L$$

The inductance and capacitance contribute to the reactance, or the imaginary component of the complex impedance, while the real component consists of the resistance. At the resonant frequency, f_0, the reactance is equal to zero and therefore the total impedance is purely resistive (Lehpamer 2008). The resonant frequency of the tag can be described by the following equation:

$$f_0= \frac{1}{2\pi\sqrt{LC}}$$

where L is the total inductance of the tag coil and C is the total capacitance. When the inductive or capacitive elements of the RFID tag are altered, the resonant frequency will change. The tag inductance is determined by the geometry of the coil, such as the dimensions, number of turns,

and thickness of each turn (Lehpamer 2008). Because these parameters were not changed during measurements with the skin patch, the observed shift in resonant frequency must be due to capacitive changes. As described in previous work by Potyrailo (2008), the dielectric properties of the substrate between the antenna turns of the coil will affect the capacitance of the RFID tag. In a dry skin patch, the coil is in contact with a thin polyurethane film and the absorbent cellulose layer. The dielectric constants of urethane and paper are 3.2 and 3.85, respectively, measured at1 kHz (Clipper Controls). The dielectric constant of water is much higher, approximately 80 at room temperature. As saline solution (99% water) is added to the cellulose layer, the dielectric constant between the tag coils should increase, resulting in a higher tag capacitance. In a separate study examining changes in the dielectric properties of paper, the capacitance of cellulose was found to increase with moisture content (Whitehead 1934). Based on the equation shown above, a higher capacitance will result in a lower center frequency of the RFID tag response. This expected decrease in center frequency was observed in RF measurements for all saline solutions and de-ionized water, allowing for the quantification of sweat present within the skin patch for volumes up to 4.5 mL. The RFID sensor response became saturated when the volume of solution added to the patch exceeded 4.5 mL, the maximum absorption capacity of the cellulose as determined in Aim 1.

Another important finding was that the shift in center frequency did not vary considerably due to the concentration of ions in the skin patch for the dilute saline solutions. When saline is added to the absorbent layer, the interaction of polar groups on the cellulose with either water or ions in solution with cellulose creates conductive pathways through the material (Whitehead 1934). While the addition of highly concentrated solution will likely affects the capacitance of the absorbent cellulose layer by competitively binding to the cellulose, human

sweat is 99% water and any contribution from the presence of ions in these experiments is expected to be small compared to the high dielectric properties of water. This will permit an accurate measurement of sweat volume in the patch independent of an individual's sweat ion content.

It was hypothesized that the conductivity of the saline solution within the sweat patch could be detected from other changes in the tag impedance spectrum. Another variable that was measured and analyzed was the bandwidth of the S11 parameter. Bandwidth increased nearly 1 MHz for solution conductivities up to around 5 mS/cm, before beginning to decrease for the more conductive solutions. The RFID tag can be described by a LCR parallel circuit, forming a bandpass filter in which the bandwidth is given by:

$$\Delta\omega = R/L$$

where R is resistance, or the real impedance, and L is the inductance. Again, because the tag inductance is a property of the coil geometry, changes in the bandwidth can be attributed to changes in the resistance of the tag. A higher tag resistance will increase the bandwidth of the reflective losses. Experimental results show a downward trend for the bandwidth as solution conductivity increased from 5 to 10 mS/cm, which may be due to decreased tag resistance from an increase in the number of conductive pathways from the ions present in solution. An interesting and unexplained observation, however, is the increase in bandwidth between the absorption of de-ionized water and diluted saline solutions. If changes in tag resistance could be attributed to the addition of conductive ions into the skin patch then bandwidth should decrease steadily as the ion content of solution is increased. Other factors, such as the competitive binding of ions and water molecules with cellulose, may be affecting the overall resistance between the antenna turns of the tag.

Changes in bandwidth were also observed as the volume of solution increased within the patch. For solutions with lower ion contents, about 20 to 40 mM sodium chloride, a sharp increase in bandwidth was observed when 1 to 2 mL of solution was absorbed by the skin patch. This point may represent the maximum amount of water molecules bound to the cellulose. As solution is added to the patch, immediate absorption and binding of water molecules to the cellulose hydroxyl groups may increase the resistance seen by the RFID tag. After the addition of about 1.5 to 2 mL of solution, exposed binding sites on the cellulose may be saturated and solution will exist freely or loosely bound within the cellulose. The increase of free ions and polar water molecules may increase the conductive pathways through the cellulose material, thus decreasing the tag resistance. It is unclear, however, why this effect would be not be observed to the same extent when de-ionized water or more concentrated saline solutions are added to the patch.

The last two variables that were measured and analyzed were the Q factor and the magnitude of reflective losses. The Q factor is a ratio of the center frequency over the bandwidth, and is therefore affected by changes in both the tag resistance and reactance. Trends in Q factor due to solution volume and conductivity represent the combined effects of center frequency and bandwidth variation, as described above. The reflected power loss is a ratio of the total power delivered to the tag to the power that is reflected back to the reader. This data is graphed in Appendix C on a logarithmic scale. The power loss measurement in decibels is related to the S11 reflection coefficient by the following expression:

$$\text{Power loss (dB)} = 20 \log |S11|$$

The ratio of reflective losses varied from .045 (.2% power reflected) in the dry patch condition to about .014 (.02% power reflected) at higher volumes of solution. The total variation in reflective

losses for both solution volume and conductivity is considerably small, and thus this parameter is not considered as a reliable indicator for sweat patch measurements with this setup.

This aim was successful in identifying a reliable measurement parameter for the radio frequency detection of saline volume within a skin patch. The magnitude of the decrease in center frequency of a passive RFID tag can be used to quantify the total volume of sweat lost over a local skin area. The second goal of this aim was to reliably detect the conductivity of solution within the patch in order to estimate electrolyte losses. No reliable marker for solution conductivity could be identified with the radio frequency setup used in these experiments. It is likely, however, that detection of solution conductivity could be accomplished with changes to the experimental setup. Previous work by Potyrailo (2010) demonstrated the feasibility of detecting buffer conductivity using passive RFID sensors with reported sensitivity of ±1.4 mS/cm for solutions between 0 and 10 mS/cm. Their setup included a barrier layer between the RFID tag and conductive solutions, and used principal component analysis to determine changes in the tag response due to solution conductivity (Potyrailo 2010). With this level of sensitivity, variation in sweat sodium content by about 25 mM should be detectable. The use of a thinner and nonporous barrier film may permit reliable detection of ion conductivity with this sensitivity. Tegaderm™ is about 90 μm thick, considerably thicker than other materials such as commercially available poly vinyl chloride plastic wrap (approximately 15 μm) or polystyrene or polypropylene films which can be as thin as hundreds of nanometers (Lock 2008). The use of these alternative sensing films to achieve more sensitive detection of ion content within the skin patch should be a topic of future research on this project.

Chapter 5: Materials and Methods

5.1 Materials

Saline solution preparation

For all experiments, 1x DPBS with calcium chloride and magnesium chloride at 7.1 pH was purchased (Invitrogen, Grand Island, NY). 1x DPBS was diluted by adding de-ionized water at 18.2 MΩ. Thirteen solutions were diluted to contain 20 to 80 mM sodium chloride, increasing in increments of 5 mM. All solutions were stored at room temperature.

Skin patch materials

Cellulose was selected as an optimal material for an absorbent skin patch for sweat collection. Five grades of nonwoven cellulose sheets from Whatman™ (GE Healthcare, Piscataway, NJ) and four grades of nonwoven cellulose sheets from Pall Corporation (Ann Arbor, MI) were obtained for absorption tests. All of the absorbent pads purchased were 100% pure cellulose fibers. Lists of the material grades, thicknesses, and absorption capacities as reported by the manufacturer are provided in Figure 1 for GE Whatman™ materials (Whatman Ltd.) and in Figure 2 for Pall Corporation materials (Pall Corp.). The nominal micron rating, shown in Figure 2 for cellulose grades from Pall Corporation, is a measure of filtration ability meaning that the majority of particles of this size will be retained by the material (DoultonUSA).

Grade	Thickness (mm)	Water Absorption Capacity (mL/cm^2)	Wicking Rate (sec/ 4 cm)
GB005	1.5	Not available	Not available
CF3	.322	.031	161
CF7	1.87	.198	35
900	1.83	.201	34
300	2.59	.240	32

Figure 1. GE Whatman™ cellulose absorbents. The reported properties of thin cellulose sheets are shown. These materials were obtained from GE Whatman™ for material testing for their potential use as the absorbent layer of a skin patch for sweat collection. (Whatman Ltd.)

Grade	Average Thickness (mm)	Nominal Micron Rating (µm)	Water Absorption Capacity (mL/cm^2)	Average Wicking Rate (sec/ 3 cm)
113	.337	3	.030	169
133	.826	18	.039	39
165	1.816	25	.161	7.9
197	2.464	14	.202	13

Figure 2. Pall Corporation cellulose absorbents. The reported properties of Pall cellulose sheets are shown. These materials were obtained from Pall Corporation to test for use as the absorbent layer of a skin patch for sweat collection. (Pall Corp.)

5.2 Cellulose Absorption

Absorption capacity

Absorption capacity is the percent by mass of liquid that is absorbed by a given material (Behery 1997). Absorption tests similar to the procedure described by the American Society for Testing and Materials (ASTM) standard D5229/D5229M-92 were performed in order to determine the absorption capacity of absorbent cellulose pads (ASTM Standard). These tests were performed first to compare the absorption capacity between different grades of cellulose materials and subsequently to assess the effect of saline concentration on absorption. Test samples measuring 2.5 cm by 2.5 cm, with a total area of 6.25 cm^2, were cut from each grade of

cellulose pad. All test samples were soaked in pure ethanol for one hour at room temperature while covered to remove any particulate matter. Samples were then placed in a humidity controlled oven at 60°C to dry for at least 12 hours. Immediately after drying, each sheet was weighed using a precision scale. This mass was recorded to four decimal places as the dry mass.

In short-term absorption tests, cellulose samples from each of the nine grades were immersed in 25 mL of saline solution diluted to 50 mM sodium chloride, as prepared above. After 10 seconds, the sample was removed from solution using tweezers and shaken lightly above solution to allow any excess saline to drip off. The sample was then blotted once on each side on a paper towel and weighed on a precision scale. The mass was recorded to four decimal places and the sample was re-immersed for an additional 10 seconds. This was repeated every 10 seconds for 90 seconds, and six times for each cellulose material grade.

To obtain absorption data over a longer time scale, new samples from each grade of cellulose were immersed in 25 mL of diluted DPBS saline at 50 mM sodium chloride. Samples were left for 10 minutes before being shaken lightly, blotted once, and weighed. Each sample was then re-immersed for an additional 10 minutes before being weighed again. This was repeated every 10 minutes for 90 minutes, and then again after 6 hours. This test was performed six times for each grade of cellulose.

Additionally, grade 165 cellulose from Pall Corporation was used to evaluate the effect of saline concentration on cellulose absorption. Both the short-term and long-term absorption tests were repeated with this material using the diluted saline solutions at 20 mM, 50 mM, and 80 mM of sodium chloride and with de-ionized water. Tests were repeated a total of six times with each solution.

For comparison of absorption between cellulose grades and saline concentrations, the absorption capacity was evaluated by determining the percent increase in mass. The percent increase in mass following immersion over an increasing time scale was calculated by the following equation:

$$\text{Increase in mass (\%)} = (m_w - m_0)/m_0 \times 100\%$$

where m_0 is the dry mass of the cellulose sample and m_w is the wet mass of the cellulose sample following immersion in solution. The maximum absorption capacity was determined from the greatest average percentage increase in mass of all measured time points. Changes in absorption capacity from 10 seconds to 6 hours of immersion were analyzed by plotting the percentage increase in mass over time.

In addition, the total amount of saline absorbed per square centimeter was used to estimate the total amount of saline that could be absorbed by a 25 cm^2 skin patch. The amount absorbed after immersion for up to 6 hours of each of the cellulose grades was determined by this equation:

$$\text{Amount absorbed (mL)} = (m_w - m_0)*(1\ \text{mL/g})*4$$

where m_0 is the dry mass of the cellulose sample and m_w is the wet mass of the sample after immersion in solution. The difference in mass is then multiplied by four to approximate the total amount of saline that could be absorbed by a skin patch with an area 25 cm^2, as cellulose samples used in this experiment were 6.25 cm^2.

Groups were maintained with n=6 independent samples for all absorption experiments. Data was plotted as the mean ± standard error using GraphPad Prism. Differences in absorption capacity between material grades and between different saline concentrations were analyzed for

statistical significance with a 95% confidence interval ($p<.05$) using a one-way analysis of variance (ANOVA).

Moisture vapor transmission rate

After determining the absorption capacities of the cellulose grades, the rate of water evaporation from saturated cellulose was examined. The moisture vapor transmission rate (MVTR) is a material property that describes the transfer of water vapor through a substrate per unit time through unit area (ASTM Standard E96/E96M). To determine the MVTR of each cellulose grade, a single 2.5 x 2.5 cm sample of cellulose was immersed in DPBS diluted to 50 mM sodium chloride for at least 24 hours. The sample was then removed using tweezers, excess saline was allowed to drip off, and the sample was blotted once on a paper towel. The sample was placed on a precision scale and left undisturbed for at least 12 hours, until all water had evaporated from the materials. The mass was recorded every 1.5 seconds for at least 12 hours.

The same procedure as described above was also used to determine if saline concentration affected water evaporation from cellulose. Samples of grade 165 absorbent cellulose pads from Pall Corporation were immersed in de-ionized water or DPBS solution diluted to 20 mM, 50 mM, or 80 mM sodium chloride before being left on a precision scale for at least 12 hours. This experiment was repeated three times for each solution.

The MVTR of the skin patch, consisting of grade 165 cellulose from Pall Corporation underneath a layer of Tegaderm™ Holding Power (HP) transparent film dressing (3M, St. Paul, MN) was also studied. Similar to the procedure described above, a 2.5 cm by 2.5 cm sample of grade 165 cellulose was immersed in DPBS solution diluted to 50 mM sodium chloride. The cellulose was removed, excess saline was allowed to drip off, and the sample was blotted once before being placed on a layer of aluminum foil on a precision scale. Tegaderm™ HP was then

placed over the cellulose sample and adhered to the aluminum foil. The cellulose and transparent dressing were left undisturbed for at least 48 hours while the mass was recorded every 1.5 seconds. As a control, evaporation from grade 165 cellulose placed on aluminum foil without a Tegaderm™ layer was tracked on the precision scale for at least 12 hours. Evaporation tests with and without a Tegaderm™ layer were each repeated three times.

Ambient temperature was maintained at 24.6 ± 1.8°C and 22 ± 3% relative humidity for the duration of the evaporation experiments. The MVTR in mL per hour over 6.25 cm^2 was determined from the slope of the linear region in a plot displaying the mass of the sample over time. MVTR with various saline concentrations are reported at the mean± standard error. The percent of water evaporated from each material was also calculated by the following equation:

$$\text{Water evaporated (\%)} = (m_0 - m_t)/ (m_0 - m_f) \times 100\%$$

where m_0 is the initial mass of the soaked material, m_t is the mass at a given time, and m_f is the final mass of the dried material. The % of water evaporated was calculated and plotted every 30 seconds for at least 12 hours, and the results were plotted over time using GraphPad Prism. Statistical analysis was performed to determine whether differences in MVTR between the cellulose grades, various saline solutions, and the presence or absence of a film dressing were significant. For this analysis, one-way ANOVA was used with a 95% confidence interval in GraphPad Prism.

Imaging of skin patch materials

Scanning electron microscopy (SEM) was used to image samples of skin patch materials to examine the microstructure of cellulose sheets following fluid absorption and to approximate the pore size and organization of transparent Tegaderm™ films. Grade 165 absorbent cellulose sheets from Pall Corporation were immersed in dilute saline solution or de-ionized water and left

to dry for at least 48 hours. All samples were sputter coated with gold at 200 Hz and 90 seconds per mA immediately prior to imaging.

5.3 Material Electrical Testing

Conductivity measurements of saline solutions

The conductivity of each diluted saline solution as well as de-ionized water was measured in Siemens per centimeter using a conductivity probe (SevenMulti, Mettler Toledo, Bedford, MA). The resistivity of each solution, in Ω•m, was calculated by taking the inverse of the conductivity.

Four-point resistivity measurements

A four-point probe setup was assembled to measure the sheet resistance of the cellulose absorbent pads prior to radio frequency measurements. Samples of cellulose sheets, grade 165, were cut into 1 cm x 2.5 cm rectangular samples and the setup shown in Figure 3 was assembled. A DC voltage source and ammeter were placed in series and connected with alligator clips to short (~3 cm) segments of copper wire. The copper wire segments were positioned upright at either end of the cellulose sample. The wires were held in place and perpendicular to the sample through small holes punched in a petri dish. Two additional segments of copper wire were then

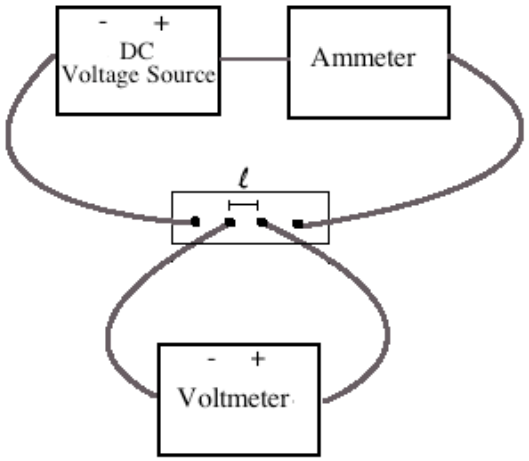

Figure 3. Four-point setup for resistivity measurements. The arrangement shown above was used to measure the electrical resistivity in cellulose sheets. Electrical contacts were made with copper wire positioned perpendicular to the cellulose sample.

attached to alligator clips and connected to a voltmeter. These two probes were placed in between the previous wires, separated by a distance of 1 cm on the cellulose sample.

Measurements were performed with samples of grade 165 absorbent cellulose following immersion in saline solution diluted to 20, 50, and 80 mM sodium chloride. Each sample was completely immersed in saline solution for at least two minutes before being removed using tweezers. Excess solution was allowed to drip off and samples were blotted once on each side before the wire leads were placed in contact with the cellulose. To determine the resistivity between the two inner leads the DC voltage source was set to supply 10 V, and the current and voltage from the ammeter and voltmeter, respectively, were recorded. Measurements were repeated at least three times with different cellulose samples immersed in each concentration of saline. The resistivity (ϱ) was later calculated by the following equation (Heaney 2000):

$$\varrho\ (\Omega \bullet m) = Vwh/Il$$

where V is the voltage measured from the voltmeter in volts, w is the width of the sample in meters, h is the thickness of the sample in meters, I is the current measured from the ammeter in amperes, and l is the distance between the two inner probes.

5.4 Radio Frequency Measurements with Saline Solutions

Experimental setup

A vector network analyzer Model 8753D from Hewlett Packard (Pao Alto, CA) was used to perform one-port scattering parameter reflectance measurements (S11 parameter). Briefly, radio waves were transmitted by the sensing coil and reflected by an RFID tag back to the sensing coil on the network analyzer. The impedance spectrum of the tag was analyzed, and the center frequency, bandwidth, Q factor, and magnitude of reflective power losses were recorded from a log chart of the S11 parameter. For all experiments, the network analyzer was set to a

frequency range of 1 to 20 MHz and an intermediate frequency bandwidth of 100 Hz. A sensing coil (diameter= 3 cm) fabricated on a printed circuit board was inductively coupled with a commercially available passive RFID tag at a resonant frequency of 13.56 MHz (RI-I11-110A-01, Texas Instruments, Waltham, MA). This operating frequency was selected because it is a lower frequency in a reserved industrial, scientific, and medical (ISM) band.

The primary coil was attached to the network analyzer using a SubMiniature version A connector with an impedance of 50 Ω. The RFID tag was then secured to the primary coil using double-sided tape placed outside the antenna coil to prevent any movement during measurements. The tag was secured so that all electrical components were facing up, away from the primary coil. A single layer of polyurethane, a Tegaderm™ HP dressing (3M, St. Paul, MN), was adhered over the RFID tag. This polymer layer was placed to serve as a protective film to reduce losses at the resonant frequency of the sensing coil in contact with a conductive medium. Once the Tegaderm™ layer was secured to the tag, a baseline measurement was taken. For each RF measurement, three plots and five values were recorded. The magnitude of the reflective power losses (dB), center frequency (MHz), bandwidth of the resonance signal (MHz), and quality (Q) factor were recorded directly from the log-magnitude plot of the S11 parameter. In addition, the log-magnitude plot, z-reflection of the real impedance, and z-reflection of the imaginary impedance were stored using MatLab for future analysis.

Radio frequency measurements within the skin patch

Samples of grade 165 cellulose absorbent sheets (Pall Corporation, Ann Arbor, MI) were cut into 5 cm by 5 cm squares and soaked in ethanol for one hour at room temperature to remove any particulate matter. Samples dried in a humidity controlled oven at 60°C for at least 12 hours. Samples were then removed from the oven and weighed using a precision scale to determine the

dry mass to four decimal places. After a baseline air measurement was recorded, the dry sample was placed on the resonant antenna and Tegaderm™ layer completely covering the sensing coil. The experimental setup used for all radio frequency measurements is diagrammed below, in Figure 4. A S11 parameter measurement with the dry patch was recorded from the network analyzer. With the dry sample still in place on the resonant antenna, .25 mL of diluted saline solution or de-ionized water was added to the center of the cellulose sample with a pipette and RF measurements were recorded. Additional aliquots of .25 mL of the same saline solution were added to the sample, and measurements were recorded after each added volume of solution. This was continued until a total of 5 mL of solution was added to the patch. After 5 mL had been added, the cellulose patch was removed and the Tegaderm™ layer was cleaned with ethanol and dried. This procedure was performed on grade 165 samples with each of the thirteen diluted saline solutions ranging from 20 to 80 mM sodium chloride as well as with de-ionized water. Radio frequency measurements were repeated twice with each of the fourteen experimental solutions.

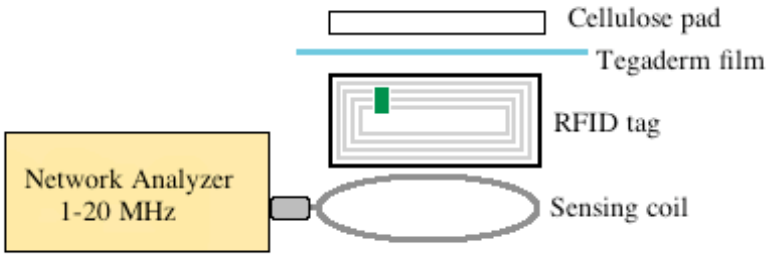

Figure 4. Radio frequency measurement setup. RF measurements following saline absorption by the skin patch were performed using the arrangement shown above. A sensing coil was using to detect changes in the impedance of an RFID tag (13.56 MHz) due to the presence of conductive saline solution in an absorbent cellulose pad. The Tegaderm film was adhered to the RFID tag to serve as a protective layer between the electrolytes and the electrical components of the tag.

The center frequency, bandwidth, Q factor, and reflective losses recorded from the magnitude chart were plotted after the addition of each .25 mL aliquot of saline solution or de-ionized water. Changes in these four parameters were taken as the difference from the dry patch and normalized to the control condition of the dry patch before the addition of de-ionized water. Data showing the change in each variable up to a total solution volume of 4.5 mL was plotted using GraphPad Prism. Statistical analysis was also performed using the analysis of variance (ANOVA) with a confidence interval of 95% ($p<.05$) in GraphPad Prism.

Changes in the center frequency, bandwidth, Q factor, and resonant losses were also examined to determine the influence of ion content on the resonance behavior of the tag. All values were taken as the difference from the dry patch condition, as above, and averaged across volumes from .25 to 2.5 mL for each of the thirteen saline solutions. Graphs of the mean ± the standard error of the mean (SEM) were plotted versus solution conductivity using GraphPad Prism. Differences due to ion content were analyzed for statistical significance using the ANOVA with a 95% confidence interval ($p<.05$) in GraphPad Prism.

Chapter 6: Conclusion

6.1 Final Comments

The work presented here describes the design and characterization of a skin patch for local sweat collection and demonstrates the feasibility of measuring sweat losses in real-time using a passive radio frequency sensor. The skin patch was designed to collect and hold sweat efficiently on the surface of the skin without affecting the secretion from the glands. The absorption capacity of the patch should match sweat rates for even the heaviest sweater for about 3 hours of total wear without saturation, which would lead to excess moisture accumulation on the skin and loss of the RFID sensor response. In addition, the rate of moisture transmission through the absorbent layer of the patch should be fast enough to lock moisture away from the skin, while the slower rate of transmission through the adhesive film cover should prevent excess evaporative losses that would skew sweat volume measurements. With an optimal skin patch design, radio frequency measurements showed that the total volume of solution within the absorbent layer could be correlated to a detectable shift in center frequency of a passive RFID tag. These results prove that an integrated skin patch and sensor system could be used to track local sweat losses in real-time, providing valuable information on an athlete's hydration status. This promising technology could allow for physiological monitoring during sports games and competitions to dramatically improve the health and performance of athletes.

6.2 Future Directions

The work presented here serves as a foundation for the development of a wearable sensor to quantify sweat losses in real-time. Additional work, however, is needed before such a device is ready for use. An appropriate next step in this project is the testing of the skin patch and integrated sensor on a model system with controlled sweat secretion. Such a model should

consist of an elastic substrate with a pore density similar to that of the skin from which pressurized saline solution could be secreted at a rate that is physiologically relevant. Testing on an *in vitro* system would be useful to more accurately characterize the RF sensor response to saline absorption. This would be an appropriate precursor to testing of the skin patch and sensor on human subjects. The electrical properties of the underlying skin may alter the background signal of the RF sensor, but these effects can likely be eliminated with proper calibration. Testing on a skin model and on human subjects will provide valuable feedback on necessary improvements to either the skin patch design, for wearability and efficient sweat collection, or the sensor integration, for accurate and sensitive detection of sweat volume. Achievement of these next steps will bring the long-term goal of this project, the development of a wearable device for sweat analysis, closer to fruition.

Appendices

Appendix A: Cellulose Absorption

This section of the appendix provides two additional graphs showing the absorption of grade 165 cellulose from Pall Corporation. The first graph shows short-term absorption, from 0 to 90 seconds of immersion in saline solution, while the second graph shows long-absorption, up to 6 hours of immersion. Absorption capacity increased steadily for longer immersion times.

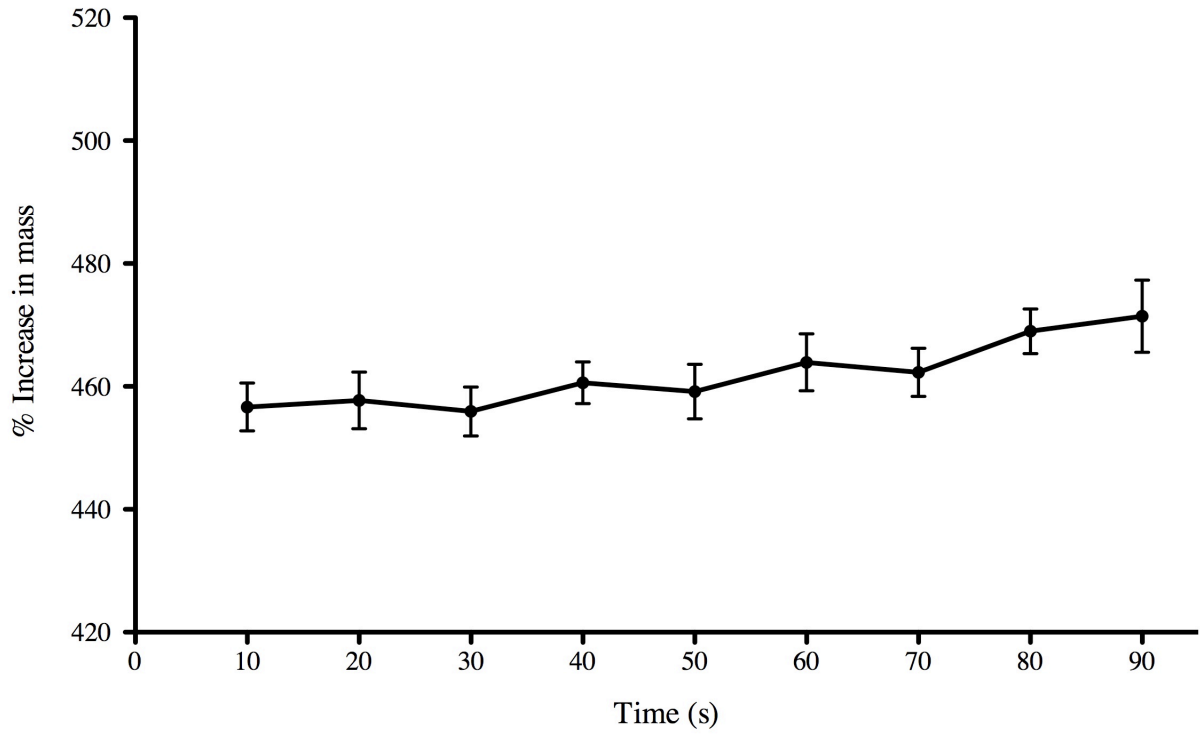

Figure 1A. Short-term saline absorption by Pall grade 165 cellulose pads. The percent increase in mass of grade 165 cellulose sheets following immersion for 10 seconds to 90 seconds in saline diluted to 50 mM sodium chloride are shown. Data is displayed as mean values ± standard error for n=6 samples. Differences in absorptive capacity between these time points are not significant (1-way ANOVA, p=.1584).

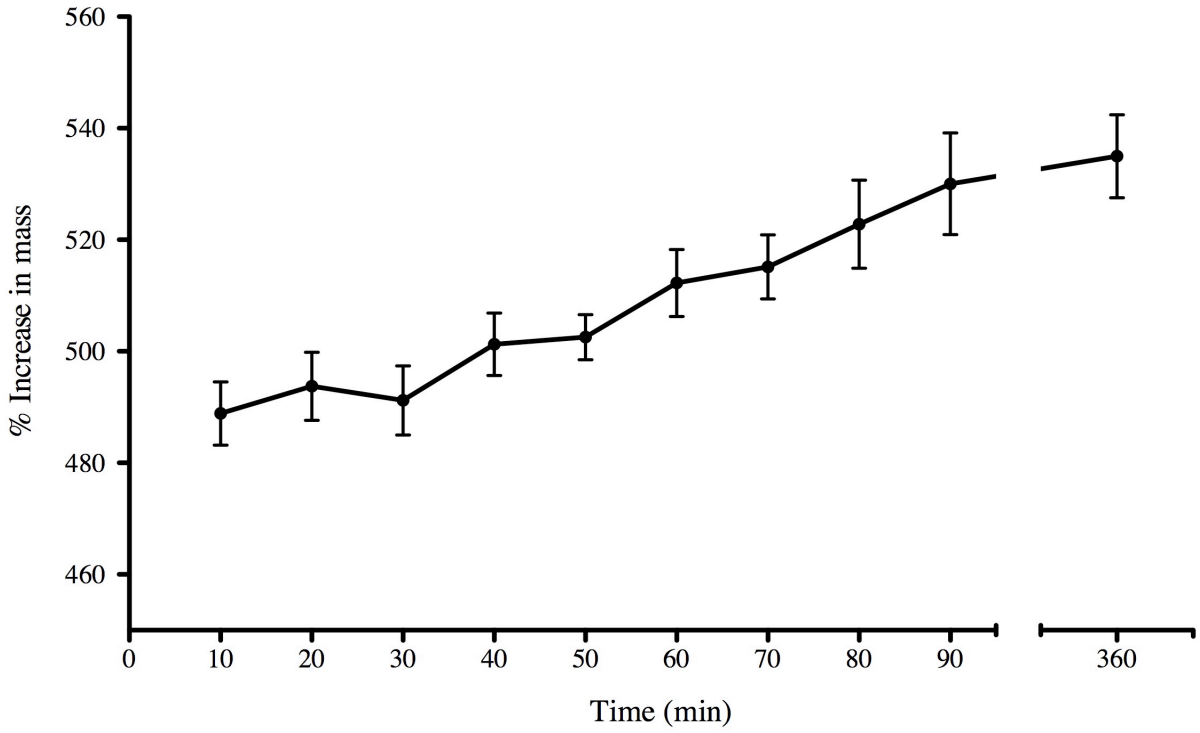

Figure 2A. Long-term saline absorption of Pall grade 165 cellulose pads. The percent increase in mass of grade 165 cellulose sheets following immersion for 10 minutes to 90 minutes and 6 hours in saline diluted to 50 mM sodium chloride are shown. Data is displayed as mean values ± standard error for n=6 samples. Variations in absorptive capacity between these time points are significant based on a 1-way unpaired ANOVA ($p<.0001$).

Appendix B: SEM Image of Tegaderm™ Film

In this section, a high-resolution image of Tegaderm™ HP from 3M™ is provided. Tegaderm™ is a transparent, adhesive film dressing made from polyurethane that is used in this project as a skin patch cover and sensing layer on the RFID tag. The object seen in the upper portion of the image is a dust particle.

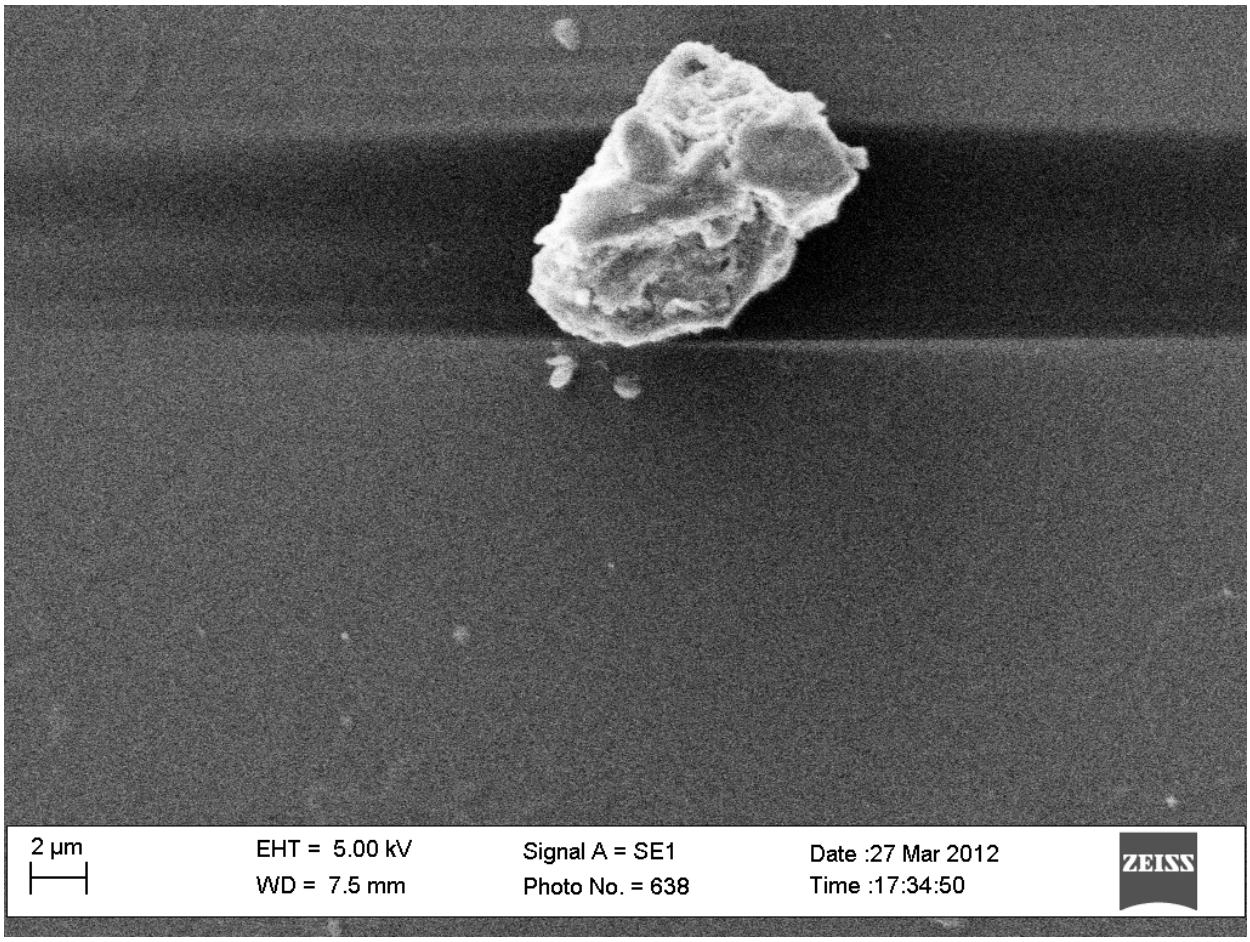

Figure 1B. SEM image of Tegaderm™ transparent film dressing. The smooth surface microstructure of unstretched 3M™ Tegaderm™ transparent film dressing is apparent from high-resolution imaging. Because material pores could not be detected here with resolution of approximately 1 µm.

Appendix C: Radio Frequency Data

Additional graphs from radio frequency measurements are provided in this appendix. The first figure shows changes in the center frequency for increasing volume of each of the saline solutions and de-ionized water. Subsequent figures display changes in Q factor due to volume and conductivity of solution, followed by changes in the reflective losses due to volume and conductivity of solution.

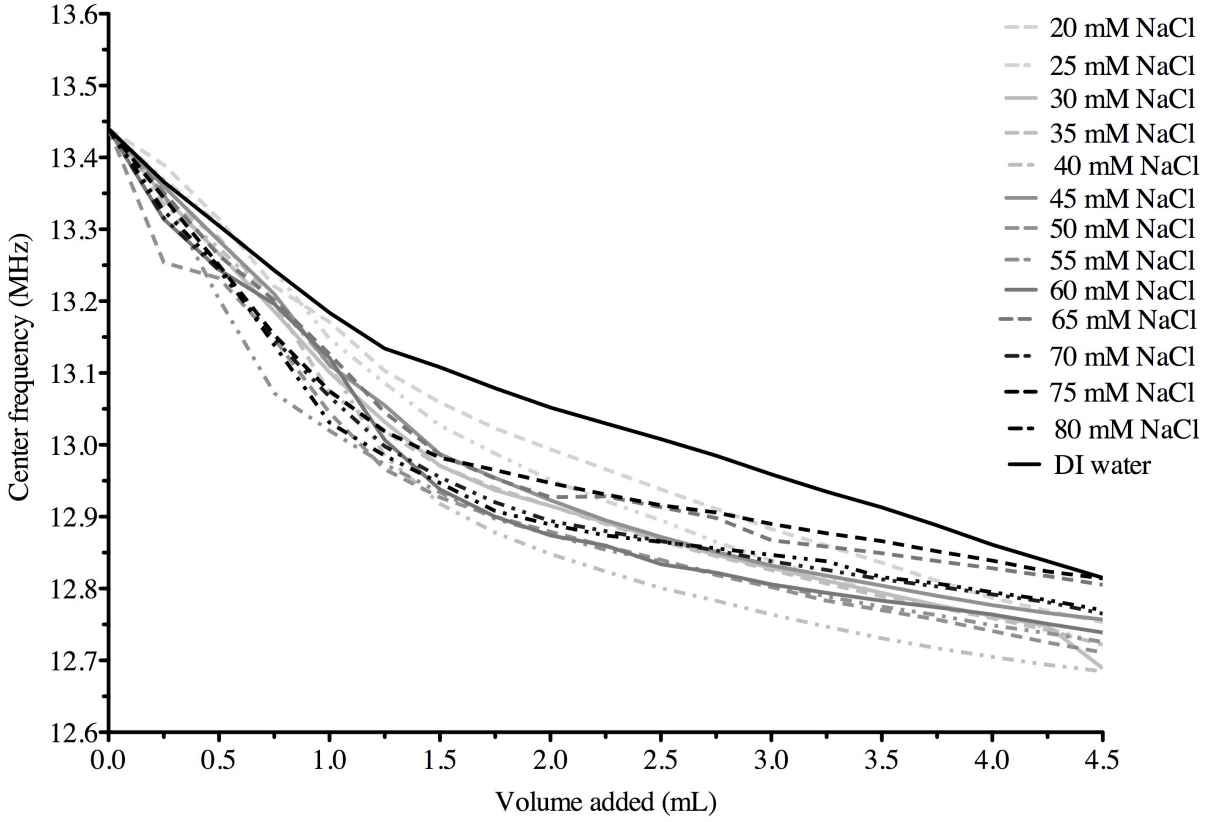

Figure 1C. Decrease in center frequency for each of the saline solutions. A decrease in center frequency of the resonance peak was seen with the addition of fluid (.25 mL) on the skin patch for each of the test solutions. Differences due to volume within the patch and ion content of the thirteen diluted saline solutions are significant based on a two-way ANOVA ($p<.0001$).

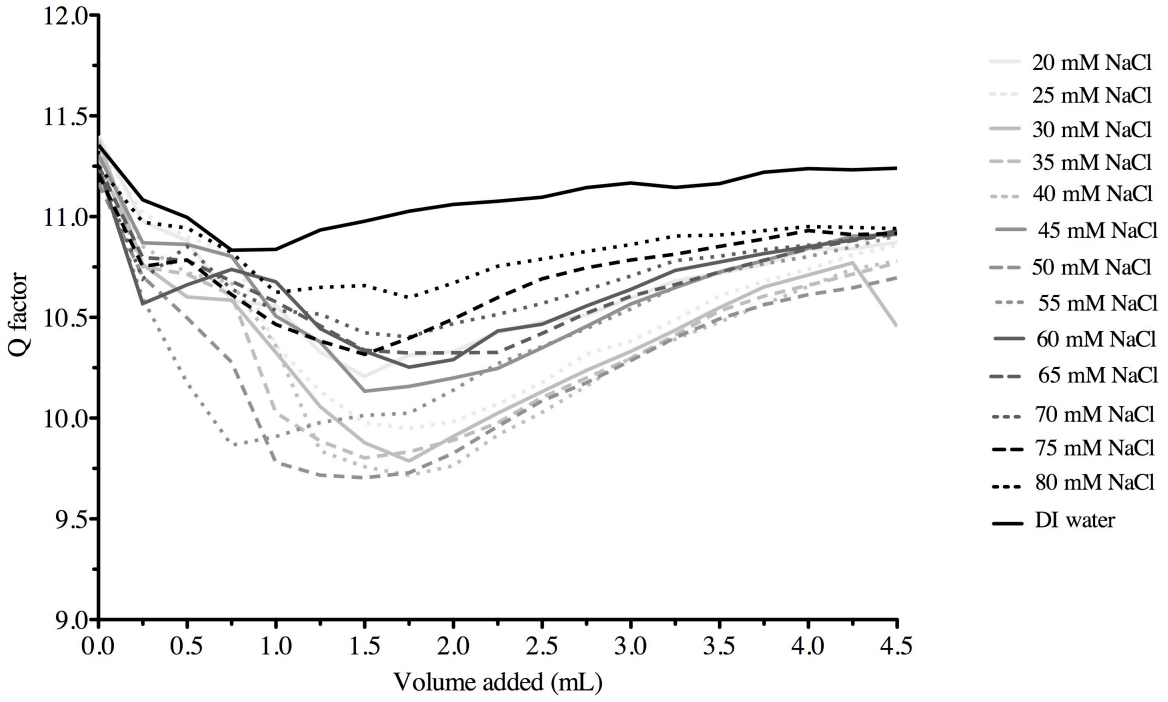

Figure 2C. Change in Q factor with saline absorption. The Q factor changed with the addition of saline solution to the skin patch. The changes observed for each of the experimental solutions are shown. Differences in Q due to volume of solution in the cellulose layer are significant (one-way ANOVA, $p<.0001$).

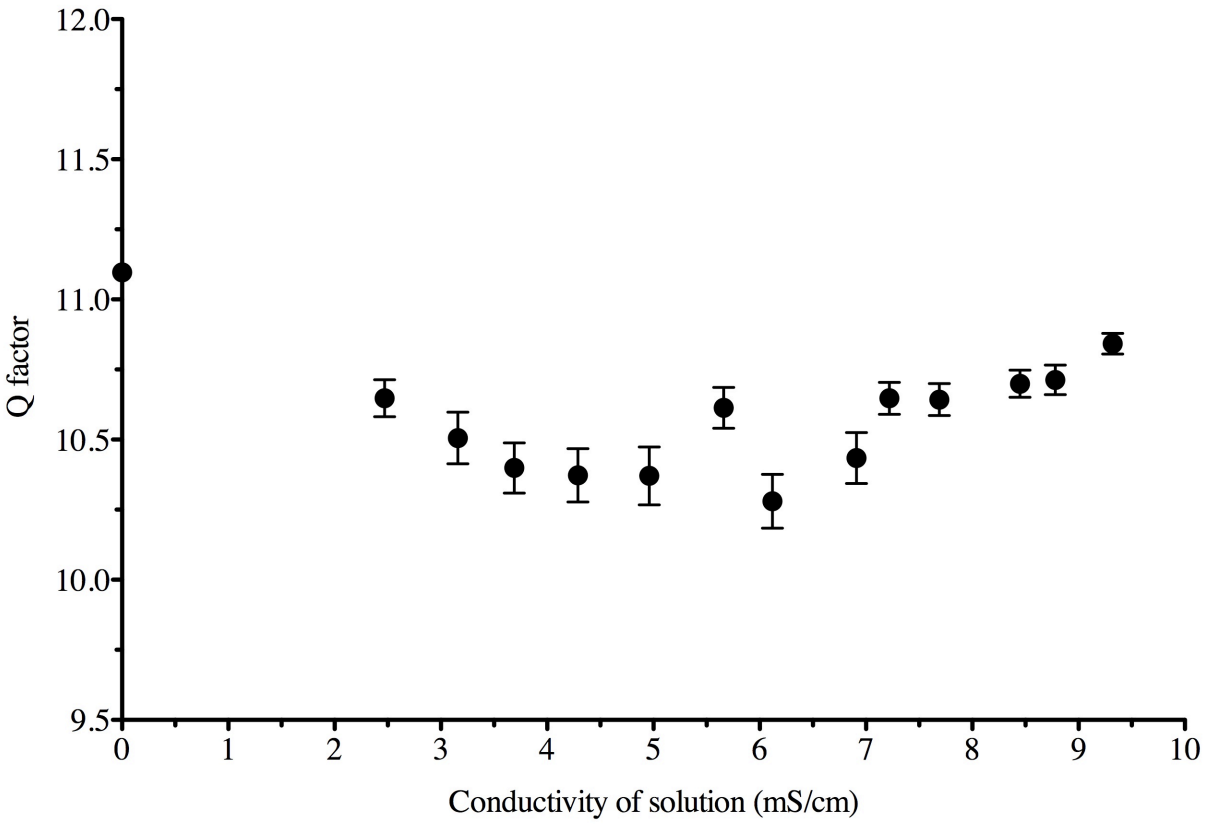

Figure 3C. Average Q factor for saline solutions. The average Q factors for the thirteen saline solutions and de-ionized water are shown as the mean ± SEM. Differences between the fourteen groups are statistically significant based on a one-way ANOVA ($p<.0001$).

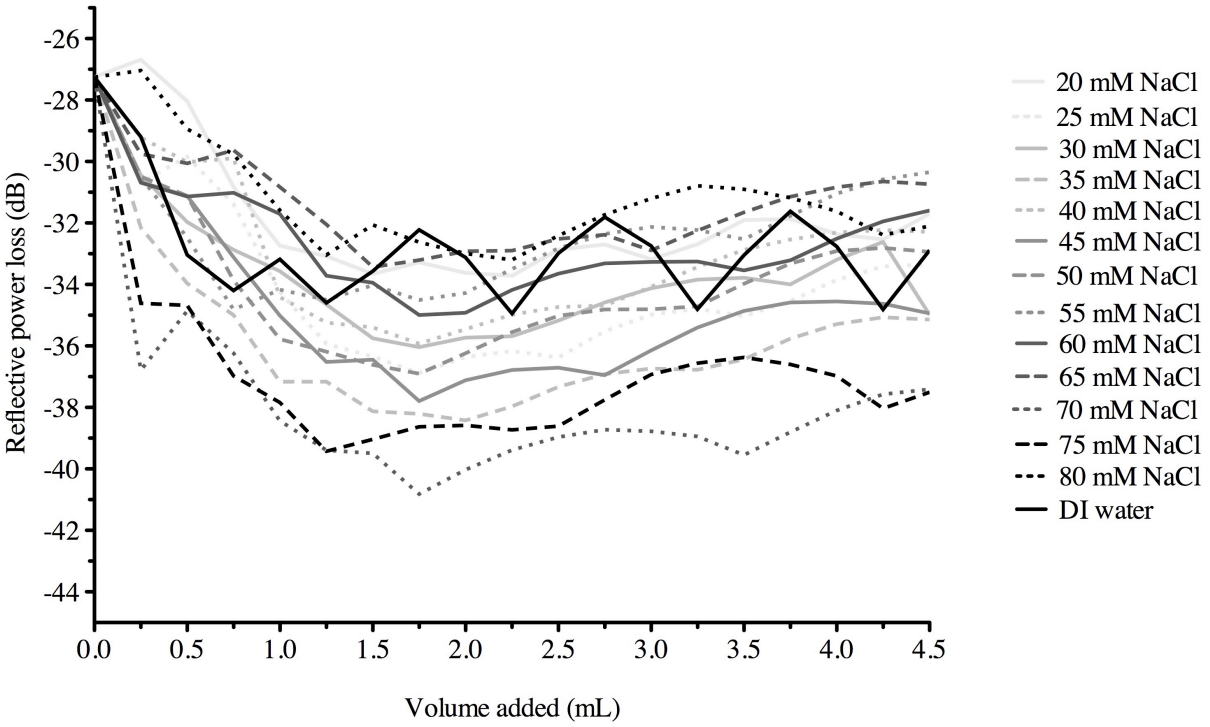

Figure 4C. Change in reflective power loss with saline absorption. The changes in the maximum reflective power losses with the addition of saline solution or de-ionized water to the skin patch are shown. Differences in power losses due to volume of solution are statistically significant (one-way ANOVA, $p<.0001$).

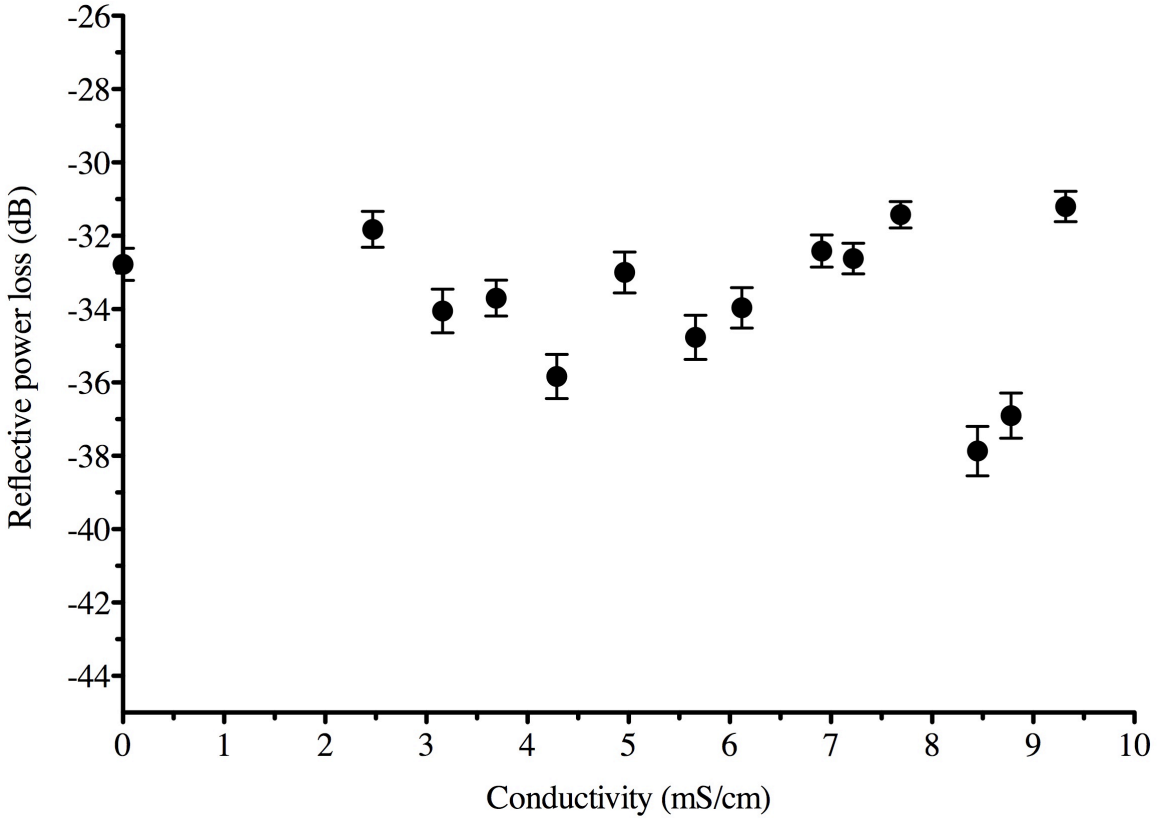

Figure 5C. Average reflective power loss for saline solutions. The average reflective power loss at resonance was calculated for the thirteen saline solutions and de-ionized water. Data is displayed as the mean ± SEM for total solution volumes from 0 to 4.5 mL, Differences in the resonant losses between solutions reached statistical significance (ANOVA, $p<.0001$).

References

Almond, C.S.D., Shin, A.Y., Fortescue, E.B., et al. 2005. Hyponatremia among runners in the Boston Marathon. *New England Journal of Medicine*. **352**: 1550-1556.

Armstrong, L.E. 2005. Hydration assessment techniques. *Nutrition Reviews*. **63**: S40-S54.

Armstrong, L.E. 2007. Assessing hydration status: the elusive gold standard. *Journal of the American College of Nutrition*. **26**:575S-584S.

ASTM Standard D5229/D5229M. 2010. Standard Test Methodology for Moisture Absorption Properties and Equilibrium Conditioning of Polymer Matrix Composite Materials. *American Society for Testing and Materials International,* West Conshohocken, PA. DOI: 10.1520/D5229_D5229M-92R10.

ASTM Standard E96/E96M. 2010. Standard Test Methods for Water Vapor Transmission of Materials. *American Society for Testing and Materials International*, West Conshohocken, PA. DOI: 10.1520/E0096_E0096M-10.

Bain, A.R., Deren, T.M., and O. Jay. 2011. Describing individual variation in local sweating during exercise in a temperate environment. *European Journal of Applied Physiology*. **111**:1599-1607.

Baker, L.B., Stofan, J.R., Hamilton, A.A., and C.A. Horswill. 2009. Comparison of regional patch collection vs. whole body washdown for measuring sweat sodium and potassium loss during exercise. *Journal of Applied Physiology*. **107**:887-895.

Behery, H.M. 1997. Characterization and testing of nonwovens with emphasis on absorbency, in *Nonwovens- Theory, Process, Performance, and Testing*, edited by Albin F. Turback. Tappi Press: Norcross, GA.

Bergeron, M. F. 2008. Muscle cramps during exercise- is it fatigue or electrolyte deficit? *Current Sports Medicine Reports*. **7**: S50-S55.

Buono, M.J., Ball, K.D., and Kolkhorst, F.W. 2007. Sodium ion concentration vs. sweat rate relationship in humans. *Journal of Applied Physiology*. **103**:990-994.

Cheuvront, S.N. and M.N. Sawka. 2005. Hydration assessment of athletes. *Sports Science Exchange 97*. **18**.

Cheuvront, S.N, Carter, R., Castellani, J.W., and M.N. Sawka. 2005. Hypohydration impairs endurance exercise performance in temperate but not cold air. *Journal of Applied Physiology*. **99**:1972-1976.

Cheuvront, S.N., Montain, S.J., Goodman, D.A., Blanchard, L., and M.N. Sawka. 2007. Evaluation of the limits to accurate sweat loss prediction during prolonged exercise. *European Journal of Applied Physiology*. **101**:215-224.

Cheuvront, S.N., Ely, B.R., Kenefick, R.W. and M.N. Sawka. 2010. Biological variation and diagnostic accuracy of dehydration assessment markers. *American Journal of Clinical Nutrition*. **92**:565-573.

Cian, C., Koulmann, N., Barraud, P., et al. 2000. Influence of variations in body hydration on cognitive function: effect of hyperhydration, heat stress, and exercise-induced dehydration. *Journal of Psychophysiology*. **14**:29-36.

Clipper Controls. Dielectric constants of various materials. *Clipper Controls Inc*. Accessed 18 April 2012. Available: http://www.clippercontrols.com/pages/Dielectric-Constant-Values.html.

Collins, K.J., and J.S. Weiner. 1962. Observations on arm-bag suppression of sweating and its relationship to thermal sweat gland "fatigue". *Journal of Physiology*. **191**:538-556.

Coyle, E.F. 2004. Fluid and fuel intake during exercise. *Journal of Sports Science*. **22:**39-55.

Deitzel, J.M., Kleinmeyer, J., Harris, D., and N.C. Beck Tan. 2000. The effect of processing variables on the morphology of electrospun nanofibers and textiles. *Polymer*. **42**:261-272.

Dobkin, D. 2008. *The RF in RFID: Passive UHF RFID in Practice*. Newnes: Oxford.

DoultonUSA. Absolute vs. nominal microns rating. *Eco Systems International LLC*. Accessed 28 March 2012. Available: http://doultonusa.com/HTML%20pages/absolute_vs_nominal_microns_rating.htm

Dove, L.L. 11 October 2010. Understanding Eccrine Sweat Glands. *HowStuffWorks.com*. Accessed 30 January 2012. Available: http://health.howstuffworks.com/wellness/men/sweating-odor/understanding-eccrine-sweat-glands.htm.

Faller, C., Bracher, M., Dami, N., and R. Roguet. 2002. Predictive ability of reconstructed human epidermis equivalents for the assessment of skin irritation of cosmetics. *Toxicology in Vitro*. **16**: 557-572.

Freudenthal, E., Herrera, D., Kautz, F., et al. 2007. Evaluation of HF RFID for implanted medical applications. *University of Texas at El Paso Departmental Technical Reports (CS)*. Paper 162, Available: http://digitalcommons.utep.edu/cs_techrep/162.

Fujimoto, S., and Watanabe, T. 1969. Studies on the body surface area of Japanese. *Acta Med Nagasaki*. **13**: 1–13.

Gopinathan, P.M, Pichan, G. and V.M. Sharma. 1988. Role of dehydration in heat stress-induced variations in mental performance. *Archives of Environmental Health*. **43**:15-17.

Grandjean, A.C. and N.R. Grandjean. 2007. Dehydration and cognitive performance. *Journal of the American College of Nutrition*. **26**:549S-554S.

Greenleaf, J.E. 1992. Problem: thirst, drinking behavior, and involuntary dehydration. *Medicine and Science in Sports and Exercise*. **24**:645–656.

Guo, Y., Li, Y., Yao, L., Liu, R., Cao, X., and M. Cao. 2011. Skin temperature, stratum corneum water content, and transepidermal water loss distributions during running. *Journal of Fiber Bioengineering and Informatics*. **4:2**53-266.

Hall, J.E. 2011. *Guyton and Hall Textbook of Medical Physiology*. Saunders: Philadelphia.

Hammond, K.B., Turcios, N.L., and L.E. Gibson. 1993. Clinical evaluation of the macroduct sweat collection system and conductivity analyzer in the diagnosis of cystic fibrosis. *Journal of Pediatrics*. **124**:255-260.

Harnett, P.R. and R.N. Mehta. 1984. A survey and comparison of laboratory test methods for measuring wicking. *Textile Research Journal*. **54**:471-478.

Heaney, M.B. 2000. Electrical conductivity and resistivity, in *The Measurement, Instrumentation, and Sensors Handbook,* edited by John G. Webster. CRC Press: Danvers, MA.

Helmenstine, A.M. 2012. On this day in science- January 6- Anselme Payen and Cellulose. *About.com Chemsitry*. Accessed 7 February 2012. Available: http://chemistry.about.com/b/2012/01/05/on-this-day-in-science-january-6-anselme-payen-and-cellulose.htm

Ichinose-Kuwahara, T., Inoue, Y., Iseki, Y. et al. 2010. Sex differences in the effects of physical training on sweat gland responses during a graded exercise. *Experimental Physiol*ogy. **95**: 1026-1032.

Iowa State University Extension. Eat to Compete: Fluids. 2011. *Iowa State University Extension*. Accessed 4 April 2012. Available: http://www.extension.iastate.edu/nutrition/sport/fluids.html.

ISO Standard 3160-2. Watch-cases and accessories -- Gold alloy coverings -- Part 2: Determination of fineness, thickness, corrosion resistance and adhesion. *International Organization for Standardization*, 2003.

King, R.M. 2003. *Biology Made Simple*. Random House Digital, Inc.

Kondo, N., Shibasaki, M., Aoki, K., Koga, S., et al. 2001. Function of human eccrine sweat glands during dynamic exercise and passive heat stress. *Journal of Applied Physiology*. **90**:1877-1881.

Lehpamer, H. 2008. *RFID Design Principles*, 1st edition. Artech House Publishers: Norwood, MA.

Lekpittaya, P., Yanumet, N., Grady, B.P., and E.A. O'Rear. 2004. Resistivity of conductive polymer-coated fabric. *Journal of Applied Polymer Science*. **92:**2629-2636.

Lock, E., Walton, S., and Fernsler, R. 2008. Polypropylene and polyethylene films on Si substrate using spin coating technique. *Naval Research Laboratory*. Report NRL/MR/6750--08-9092.

Machado-Moreira, C.A, Caldwell, J.N., van den Heuvel, A.M.J., et al. 2009. Sweating and skin blood flow changes during progressive dehydration. *Proceedings of the 13th International Conference on Environmental Ergonomics*. 208-211.

Marcus, Y. 1988. Ionic radii in aqueous solutions. *Chemical Reviews*. **88**:1475-1498.

Maughan, R.J. and S.M. Shirreffs. 1998. Fluid and electrolyte loss and replacement in exercise, in *Oxford Textbook of Sports Medicine*, 2nd edition, edited by Harris, Williams, Stanish, and Micheli. Oxford University Press: New York.

Maughan, R.J. 2003. Impact of mild dehydration on wellness and on exercise performance. *Eur. J. Clin. Nutr*. **57**: S19-S23.

Mayo Clinc. Hyponatremia: Symptoms. 9 June 2011. *Mayo Foundation for Medical Education and Research*. Accessed 13 December 2011. Available: http://www.mayoclinic.com/health/hyponatremia/DS00974/DSECTION=symptoms

McTigue, N.E. and J.M. Symons. 2010. *The Water Dictionary: A Comprehensive Reference of Water Terminology*, 2nd edition. American Water Works Association: Denver.

Medina, J., Fraissinette, A. B., Chibout, S., et al. 2000. Use of human skin equivalent Apligraf for in vitro assessment of cumulative skin irritation of topical products. *Toxicology and Applied Pharmacology*. **164**: 38-45.

Murray, B. 2007. Hydration and physical performance. *Journal of the American College of Nutrition*. **26**:542S-548S.

Nadel, E.R., Fortney, S.M., and C.B. Wenger. 1980. Effect of hydration state on circulatory and thermal regulations. *Journal of Applied Physiology*. **49**:715-721.

O'Connor, R.E. 2006. Exercise-induced hyponatremia: causes, risks, prevention, and management. *Cleveland Clin. J. Med*. **73**: S13-S18.

Pall Corporation. Absorbent Pads. 2012. *Pall Corporation*. Accessed 11 April 2012. Available: http://www.pall.com/main/OEM-Materials-and-Devices/Product.page?id=3895.

Patterson, M.J., Galloway, S.D.R., and M.A. Nimmo. 2000. Variations in regional sweat composition in normal human males. *Experimental Physiology*. **85**:869-875.

Popowski, L.A., R.A. Oppliger, G.P. Lambert, R.F. Johnson, A.K. Johnson, and C.V. Gisolfi. 2001. Blood and urinary measures of hydration during progressive acute dehydration. *Medicine and Science in Sports and Exercise*. **33**: 747-753.

Potyrailo, R.A. 2009. Chemical sensors: new ideas for the mature field, in *Functional Thin Films and Nanostructures for Sensors*, edited by A. Zribi and J. Fortin. Springer: New York.

Potyrailo, R.A. 2010. Integration of passive multivariable RFID sensors into single-use biopharmaceutical manufacturing components. *IEEE RFID*. 1-7.

Sawka, M.N. and E.F. Coyle. 1999. Influence of body water and blood volume on thermoregulation and exercise performance in the heat. *Exercise and Sports Science Review*. **27**:167-218.

Sawka, M.N., Burke, L.M., Eichner, E.R., et al. 2007. Exercise and Fluid Replacement. *Journal of the American College of Sports Medicine*. **39**: 377-390.

Shirreffs, S.M., and R.J. Maughan. 1997. Whole body sweat collection in humans: an improved method with preliminary data on electrolyte content. *American Journal of Physiol*ogy. **82**: 336-341.

Smith, C.J. and G. Havenith. 2011. Body mapping of sweating patterns in male athletes in mild exercise-induced hyperthermia. *European Journal of Applied Physiology*. **111**:1391-1404.

Steffen, T., Luechinger, R., Wildermuth, S. et al. 2010. Safety and reliability of radio frequency identification devices in magnetic resonance imaging and computed tomography. *Patient Safety in Surgery*. **4**:2-11.

Stofan, J.R., Zachwieja, J.J., Horswill, C.A., Murray, R., Anderson, S.A., and E.R. Eichner. 2005. Sweat and sodium losses in NCAA football players: a precursor to heat cramps? *International Journal of Sport Nutrition and Exercise Metabolism*. **15**:641-652.

Swatloski, R.P, Spear, S.K., Holbrey, J.D., and R.D. Rogers. 2002. Dissolution of cellulose with ionic liquids. *Journal of American Chemical Society*. **124**:4974-4975.

Wang, X., Weilin, X., Li, W., and W. Cui. 2009. Study on the electrical resistance of textiles under wet conditions. *Textile Research Journal*. **79**:753-760.

Weschler, L.B. 2008. Sweat electrolyte concentrations obtained from within occlusive coverings are falsely high because sweat itself leaches skin electrolytes. *Journal of Applied Physiology*. **105**:1376-1377.

Whatman Ltd. Absorbent sinks. 2009. *GE Healthcare*. Accessed 6 February 2012. Available: http://www.whatman.com/PRODAbsorbentSinks.aspx.

Whitehead, J.B. and E.W. Greenfield. 1934. Dielectric properties of cellulose paper-I. *Transactions of the American Institute of Electrical Engineers*. **53**:1389-1396.

Wilke, K., Martin, A., Terstegen, L., and S.S. Biel. 2007. A short history of sweat gland biology. *International Journal of Cosmetic Science*. **29**:169-179.

Wilson, M.M., and J.E. Morley. 2003. Impact of mild dehydration on wellness and on exercise performance. *European Journal of Clinical Nutrition*. **57**: S24-S29.

Wilson, T.E., Monahan, K.D., Fogelman, A., et al. 2010. Aerobic training improves *in vivo* cholinergic responsiveness but not sensitivity of eccrine sweat glands. *Journal of Investigational Dermatology*. **130**:2328-2330.

Wu, P.C., Jones, G., Shelley, C., and B. Woelfli. 2007. Novel microporous films and their composites. *Journal of Engineered Fibers and Fabrics*. **2**:49-59.

Yu-Shuang, L., Jiong, C., Qiang, L., and P. Ke-Ping. 2009. Moisture vapor transmission rates of various transparent dressings at different temperatures and humidities. *Chinese Medical Journal*. **122**:927-930.